AEROSPACE ENGINEERING DEPARTMENT
CALIFORNIA POLYTECHNIC STATE UNIVERSITY
SAN LUIS OBISPO, CA
2011-2012

The Architecture Selection, Design, and Discharge Modeling of a Passive Compensation, Iron-Core, Two-Phase, Permanent Magnet Compulsator to Power a Small Railgun Platform

By: Collin MacGregor - ctmacgre@calpoly.edu

Faculty Advisor: Dr. Kira Abercomby
December, 2012

Abstract

The goal of this project was to design and build a compensated pulsed alternator, or compulsator, to power the Cal Poly Electromagnetic Railgun Mark 1.1. This project examines the feasibility of implementing mechanical pulsed power supplies for repeatable use with a railgun load for orbital debris hypervelocity testing. The final system architecture chosen was a passively compensated, iron-core, 2-phase, permanent magnet compulsator. The Cal Poly Compulsator will be capable of storing 45 kJ of mechanical energy with a peak operating speed of 5,000 rpm at 190 V. Theoretical calculations resulted in the following predicted electrical performance values: a peak output current discharge of 33 kA, peak output power of 3.3 MW, and a pulse width of 4.3 ms. These values result in moving a 1 g projectile to a final velocity of 410 m/s. Experimental testing and comparison will occur once the system has been assembled. The architecture selection process, description of the mathematical modeling of the system, the mechanical design, and some of the manufacturing processes undertaken during this project are included in the discussion. This paper serves as a compilation of introductory information to assist individuals who are just starting their research into compulsators.

Table of Contents

Table of Figures

Table of Tables

Acknowledgements

I would like to thank my advisor Dr. Kira Abercromby for her support as faculty adviser throughout the project. I also would like to particularly acknowledge Jeff Maniglia, without both his initial work on the Cal Poly EMRG and support during this project all of this would not have been possible. I would like to thank my original partner in this endeavor, Nolan Uchizono for helping start this project with me and his work on the project.

Most importantly, I would like to give a great big thank you to all the members of the Cal Poly Compulsator Team: Anthony Miller (B.S. ME ‘12), Erik Pratt (B.S. ME ‘12), John Terry (B.S. ME ‘12), Bryan Bennett (B.S. EE ‘12), John O’Hara (B.S. EE ‘12), and Nolan Uchizono (B.S. EE ‘12). I know that this was a very difficult and time consuming project; all of your work was greatly appreciated. There is no way we would have gotten this far without all of your contributing efforts on the project on this complicated system. Finally, I would like to thank all of my family, friends, and mentors who have provided support in your own various ways throughout my time at Cal Poly.

Nomenclature

B = field strength density (T)
D_r = diameter of rotor (m)
D_w = diameter of winding wires (m)
dI = change in output current over time (A/s)
dt = finite time step (s)
dx = particle velocity in railgun (m/s)
d^2x = particle acceleration in railgun (m/s^2)
du = state space derivative placeholder
$d\omega$ = angular acceleration of rotor (rad/s^2)
E_r = mechanical energy stored in rotor (J)
I = compulsator discharge current (A)
J_r = rotor inertia (kg-m^2/rad^2)
L = inductance (H)
L' = inductance gradient of railgun rails (H/m)
L_{min} = minimum inductance of compulsator (H)
L_{max} = maximum inductance of compulsator (H)
L_o = inductance of connecting busbar (H)
l_{cmttr} = length from rotor edge to commutator (m)
l_{turn} = length of windings based on number of turns (m)
l_{phase} = total length of a winding for one phase with two slots (m)
l_r = length of rotor (m)
m = mass of projectile (kg)
N_{cp} = number of conductors per pole on rotor
N_p = number of poles in rotor
N_{pairs} = number of pole pairs
N_t = number of turns for a winding
P_{max} = peak discharge power (W)
R' = resistance gradient of railgun (Ω/m)
R_{rg} = resistance of railgun (Ω)
R_c = compulsator internal resistance (Ω)
R_o = resistance of connecting busbar (Ω)
RPM = rotations per minute
R_{ac} = AC Resistance for Skin Effect (Ω)
t = time (s)
u = state space placeholder
V = instantaneous voltage of system (V)
V_o = rotational electromagnetic voltage (V)
v_p = projectile velocity (m/s)
v_{tip} = rotor tip speed (m/s)
X_{rg} = railgun barrel length (m)
x = projectile position along railgun (m)
δ = AC skin depth (m)
δ_e = electrical phase angle (rad)
δ_s = skin depth (m)
Φ = Flux linkage (V-s)
ρ = resistivity (Ω/m)

ρ_c = compulsator inductance modulus
ω = angular velocity (m/s)
ω_m = mechanical angular velocity (rad/s)
ω_e = electrical frequency (s^{-1})

1.0 Introduction

1.1. Project Background & Purpose

Cal Poly Pulsed Power (CPPP) is an interdisciplinary organization of students at Cal Poly who are interested in advancing research of pulsed power. The main research program within the organization focuses on the development of a hypervelocity impact testing program at Cal Poly. The goal of this test program is to recreate the orbital debris environment at geosynchronous orbit by accelerating small projectiles (1-6g) to speeds of 2-3 kilometers per second and impacting test surfaces comprising of common spacecraft materials and coatings. Follow up space environments testing will occur in vacuum chambers in a lab at Cal Poly operated by the Aerospace Engineering Department. The design and construction of a compulsator is to examine mechanical pulsed power supplies for this test program as opposed to the capacitive pulsed power supplies that are either already in use or planned for future railgun designs.

1.1.1. Orbital Debris

Orbital debris, or space junk, and the hazards it imposes on spacecraft is a major concern within the Aerospace Industry. Sources of orbital debris include: the expended upper stages of launch vehicles, decommissioned satellites, occasional collisions between spacecraft, and micrometeorite impacts [1]. Impacts from space junk or micrometeorites that are smaller than 1cm in diameter are mitigated by employing protective shielding to the spacecraft. Various methods exist for tracking pieces of space junk greater than 10cm in diameter through optical and radio measurements [1]. These objects are tracked on the ground, and are generally avoided by maneuvering active spacecraft out of the way. However, the accuracy of these methods falls off greatly for objects smaller than 10cm, which cannot be safely stopped with current shielding methods.

In order to provide sufficient shielding for spacecraft, significant research is necessary for the development of lightweight, impact-resistant shields. NASA and other space agencies have invested a lot

of research in the study and design of micrometeoroid debris shields. A costly bottleneck in this process is the testing and validation of these shields. Traditional hypervelocity impact testing is handled at facilities that have a Light Gas Gun (LGG). LGG's hyper-compress a working gas to propel a particle to orbital speeds (approximately 1-10 km/s). These facilities require extensive infrastructure to maintain, creating a significant cost barrier for debris shield testing. Additionally, a lot of testing components are consumed during each firing which adds to the cost of LGG testing.

1.1.2. Electromagnetic Railguns

Electromagnetic railguns (EMRG) are a promising alternative to the LGG approach for hypervelocity impact testing. Typical EMRG research has focused primarily on applications involving military platforms; orbital debris testing is a relatively new application for this field. An EMRG requires a fraction of the total cost and occupied space of an LGG, making an economical option for hypervelocity impact testing. The feasibility of this concept was introduced last with the successful demonstration of the Cal Poly EMRG Mk.1, which was powered by a pulsed power supply comprising of a 16 kJ capacitor bank [2]. A one gram particle was successfully accelerated to 450 meters per second during Spring Quarter 2011. The team was able to achieve these results within a budget of $5,000.

EMRGs require a large amount of energy to be pulsed over a very short time span, their power sources are referred to as pulsed power supplies. Pulsed power is a small, but growing, field within Electrical Engineering. Pulsed power involves the accumulation of massive amounts of energy (kJ-GJ range) and releasing it over an extremely short period of time. Pulsed power technology is commonly used in radar, particle accelerators, fusion research, high-power pulsed lasers, ultra-strong magnetic fields, and electromagnetic pulses [3]. There are four methods of energy storage in pulsed power: capacitive, inductive, mechanical, and chemical. In the field of pulsed power, the two most common forms of energy storage are capacitive and mechanical.

Capacitive systems are relatively inexpensive, require only fundamental knowledge of electrical components and circuitry, but have a relatively low energy density. Most capacitive systems consist of a capacitor bank, a switching system or pulse formation network, and the load. Their simplicity and low cost are the tradeoffs for their relatively low energy density.

1.2. Compulsators

1.2.1. Principle of Operation

A compensated pulsed alternator, or compulsator, is a specialized form of alternator whose primary design goal is to maximize power generation. It achieves this by having a high current carrying capability and minimizing the internal impedance of the device [4]. A compulsator works by storing its energy using inertial energy storage, converting this to electromechanical energy. A triggering switch then delivers the high power output to an external load over a short (ms to μs) timespan [5]. Similar to a traditional alternator, voltage is produced by the relative motion of a multi-pole armature and electromagnetic field. Higher voltage can be obtained by increasing the relative speed between the two components, increasing the length of the armature, or using multi-turn windings. However, the top speed of the machine is typically limited by material strength of the rotating element. Magnetic field strength is dependent on the saturation level of ferromagnetic materials, or by current density of the excitation winding conductors. Also, multi-turn windings can increase the internal impedance of the machine which limits any gains in current output that might be achieved [4].

The compulsator can also be thought of as a synchronous generator that is intentionally designed to maximize short circuit current output by minimizing internal impedance through the action of flux compression [3]. As the inertial energy storage component of a compulsator rotates, the mutual inductance between the stationary and rotating portions cause the inductance of the machine to vary over time. This cyclic variation of inductance compresses the magnetic flux generated by the load current and alters the shape of the output current pulse [6]. Flux compression occurs through the use of

special internal compensating windings that fall into one of three categories: passive, selective-passive, or active compensation [3].

1.2.2. Historical Background

In the late 1970s there was significant interest in developing new technologies in pulsed power for energy storage and power delivery. Lawrence Livermore National Laboratory (LNLL) was developing a laser fusion facility that had a need for high power, short duration electrical pulses. Capacitor banks were found to be unable to provide repetitive, high-current pulses that were required for their research. This led to the concept of a compulsator and its subsequent patenting in 1978 [5]. An engineering prototype was developed at the University of Texas at Austin Center for Electromechanics for LNLL [7, 4].

During the 1980s significant research into electromagnetic launch (EML) began with railguns. After the successes seen with the LNLL fusion experiment, it became very clear that compulsators would prove to be an effective power supply for EML. The US Army who was looking into railgun technology as a possible next-generation weapons platform on tanks. As with the fusion experiment, capacitors proved to be too unwieldy of a power supply for a mobile platform. Significant research was undertaken at the Center for Electromechanics, University of Texas at Austin into the feasibility of railgun platforms for future weapon systems. The Electromagnetic Gun Weapons System program was created to demonstrate the advantages of electromagnetic weapons for armor penetration. Several systems were developed to examine the feasibility of EML for weapon platforms [4, 8]. Present-day compulsator research is very active in China where research involves placing compulsators on amphibious assault vehicles to power next-generation EML weapon platforms [9].

1.2.3. Compulsator Topologies

There are many design architecture decisions that must be made when examining the implementation of a compulsator system for a pulsed power application. Since their inception in 1978,

compulsator systems have gone through five generations of different technological advances at UT Austin CEM alone [3]. There are several major components in the topology of a compulsator that can be varied depending on the requirements of the system [4]:

- Excitation windings or another method of magnetic field generation
    - This generates the magnetic field in the system
- Compensation scheme, and subsequent compensation windings or shield
    - This dictates the output current waveform shape
- The type of rotating element
    - Source of inertial energy storage and typically houses the armature windings

The decisions made on the above compulsator topologies will affect the entire system as a whole. A compulsator can be broken down into the following major elements:

1. Excitation windings
2. Armature windings, which interact with the excitation windings to generate voltage
3. Compensation winding or shield
4. Rotor
5. Stator
6. Bearings
7. Brush mechanisms, which deliver power from the compulsator into the switching circuitry and the external load
8. Support structure

Additionally, there are several discrete decisions that must be made when designing a compulsator system to meet the requirements and parameters for a pulsed power mission. These decisions are directly related to the different compulsator topology elements already mentioned. Further discussion on these different options will be handled in the following section, a diagram [3] depicting the different design options available for current compulsators is included below:

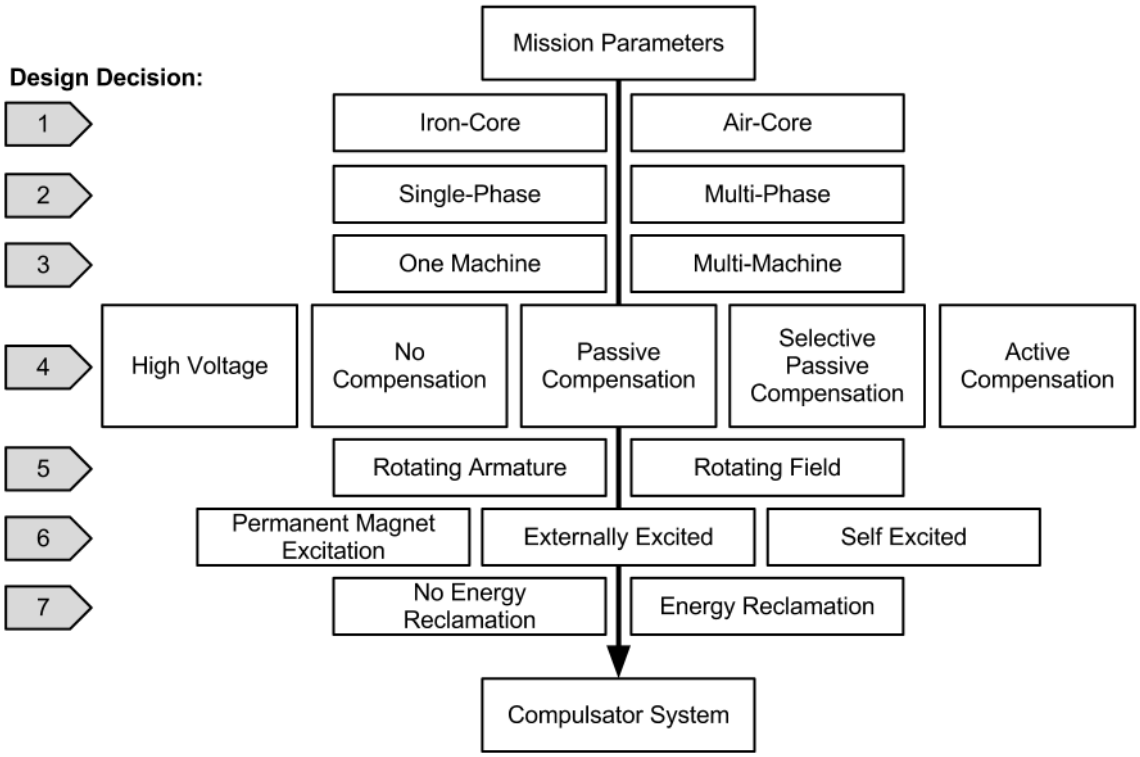

Figure 1: Compulsator architecture decision tree [3] showcasing the different design options that must be considered for a complete compulsator system.

1.2.3.1. Core Topology Options

There are two options for core topology in a compulsator: iron-core and air-core magnetic circuits [10]. Iron-core machines have a higher magnetic permeability, and tend to be considerably more magnetically efficient than air-core machines. Because of the low specific strength and high density of ferromagnetic materials severely limits the maximum rotor tip speed, placing upper limits on the energy storage density of iron-core machines [10]. The excitation flux densities of iron-based alloys typically ranges close to ~1.8 T, and serve as a material property cap for iron-core compulsators, except in the case of expensive, high saturation iron materials where flux densities can be increased to just above 2 Tesla [10]. Iron-core machines are typically more robust than air-core machines, but their delivered energy density is lower because they are a less energy-dense system [3]. Complex field winding schemes are difficult to implement in iron-core machines because of machining limitations as field windings in an iron-core machine are typically placed in slots.

As energy density and power delivery requirements rise, optimizing compulsators for maximum energy storage and power density favors air-core machines for two primary reasons [10]. The use of high strength, low density composite materials allows for operation at rotor tip speeds two to three times higher than what is possible in iron-core machines [3, 10]. Unlike the magnetic saturation limit on iron-core machines, air-core compulsators can be optimized to operate at significantly higher flux densities. This allows for required voltages to be reached with fewer armature turns, which lowers the overall resistance of the machine [10]. Additionally, the lack of ferromagnetic materials in the core further reduces the internal inductance of the machine, leading to lower overall impedance in the system. Most air-core machines typically have self-excited magnetic fields, see section 1.2.3.6., and have an overall efficiency penalty in establishing the excitation field [10]. Air-core machines allow for parameters like rotor tip speed, excitation flux density, and efficiency to be optimized to provide a minimum weight and volume compulsator for a given duty cycle [10].

1.2.3.2. Output Phase Options

Early compulsators were all configured as single-phase machines, where the required current pulse came from a single voltage cycle. This design approach simplifies the output switch requirements; however it does require the desired output pulse duration to be close to the voltage period provided by the fundamental machine electrical frequency [10]. To minimize the physical size of a single-phase machine with a given stored energy requirement, the number of poles must be minimized to increase rotational speed. Reducing the size of a compulsator is important since less material is required and affects the overall system cost. There is a practical limit at two-pole configurations, where a variety of electromagnetic and mechanical problems such as arcing can arise [10]. The single-phase machine has a natural current zero and passive energy recovery from the railgun [3]. Electromagnetic field compensation schemes allow for further manipulation of the output pulse waveform, see section 1.2.3.4.

Multi-phase machines offer more flexibility in current waveform shaping [3]. These compulsators utilize a higher electrical frequency than single-phase machines. Since there are multiple phase outputs in a multi-phase machine, the entire output is rectified to provide the required pulse width and shape. Output waveform shaping removes the pulse duration and electrical frequency limitations experienced by single-phase machines [10]. This allows for the number of poles and the rotational speed of the rotor to be separately optimized to reach desirable parameters: high numbers of poles and high angular velocity, thus increasing the energy density of the system. Careful analysis and trades must still be made between machine size, switching hardware size, system mass, and cost [10].

Another major consideration in the multi-phase system architecture is the type of rectifier. A full wave, phase-controlled rectifier allows for the greatest pulse shaping capability. However, this requires approximately twice the number of switching devices as a half-wave, phase controlled rectifier because current flows in each bridge leg at all times [10].

1.2.3.3. Single Machine vs. Multi-machine Systems

EML system can have very high delivered energy requirements in the Mega-ampere range, with Gigawatts of output power [11]. As performance requirements increase, compulsator design becomes more technically challenging to meet. Benefits can be seen in a system where the overall delivered energy is distributed across multiple, identical compulsators instead of a single specifically designed machine. The outputs of multiple compulsators would be combined in parallel to the load to meet performance requirements. Most EML systems are designed for use on mobile platforms; in this case, two smaller pulsed alternators could be configured to rotate in opposite directions to counteract induced effects of angular momentum that might negatively impact the operation of a mobile platform. Distributing energy delivery requirements across multiple compulsators is particularly useful for applications involving armored combat vehicles, or for space-based railgun applications. Introducing a

mass-producible compulsator system that could be modularly configured in parallel could be an intriguing commercial concept for future pulsed power applications.

1.2.3.4. Compensation Schemes

The main difference between compulsators and conventional alternators is through the use of compensation. Compensation reduces armature inductance through compensating currents which limit the volume occupied by the armature-produced fields [4]. To maximize the effect of inductance reduction, currents of equal magnitude and opposite sense flow in a conductor that is located physically close to the armature [4]. The total magnetic flux produced by the armature is reduced, and the fields are then contained between the armature and compensating conductors [4]. A common example is the coaxial cable, where the inductance is a function of the ratio of the radii of the two conductors. In the case of compulsators, opposing currents flow on the outer surface of the rotor and the inner surface of the stator bore [4]. To lower inductance, the magnetic air gap between the opposing currents and the thickness of conductors are minimized. Because a compulsator is a multi-pole machine, the degree of compensation depends on the relative alignment of the armature and compensating poles [4]. This can lead to an inductance that varies with rotor position, manipulating the inductance variation is the primary method of achieving a desired pulse shape and increasing output power through flux compression [4, 6]. Compensation is also useful for limiting the armature reaction in ferromagnetic machines, and protecting the excitation windings from armature-discharge-induced transients [4]. Listed above in Figure 1 are the five different approaches to compensation for electromechanical power supplies. High voltage machines without compensation typically cover niche aspects in compulsator output performance. Compulsators have three possible compensation schemes available to them: passive, selective passive and active compensation.

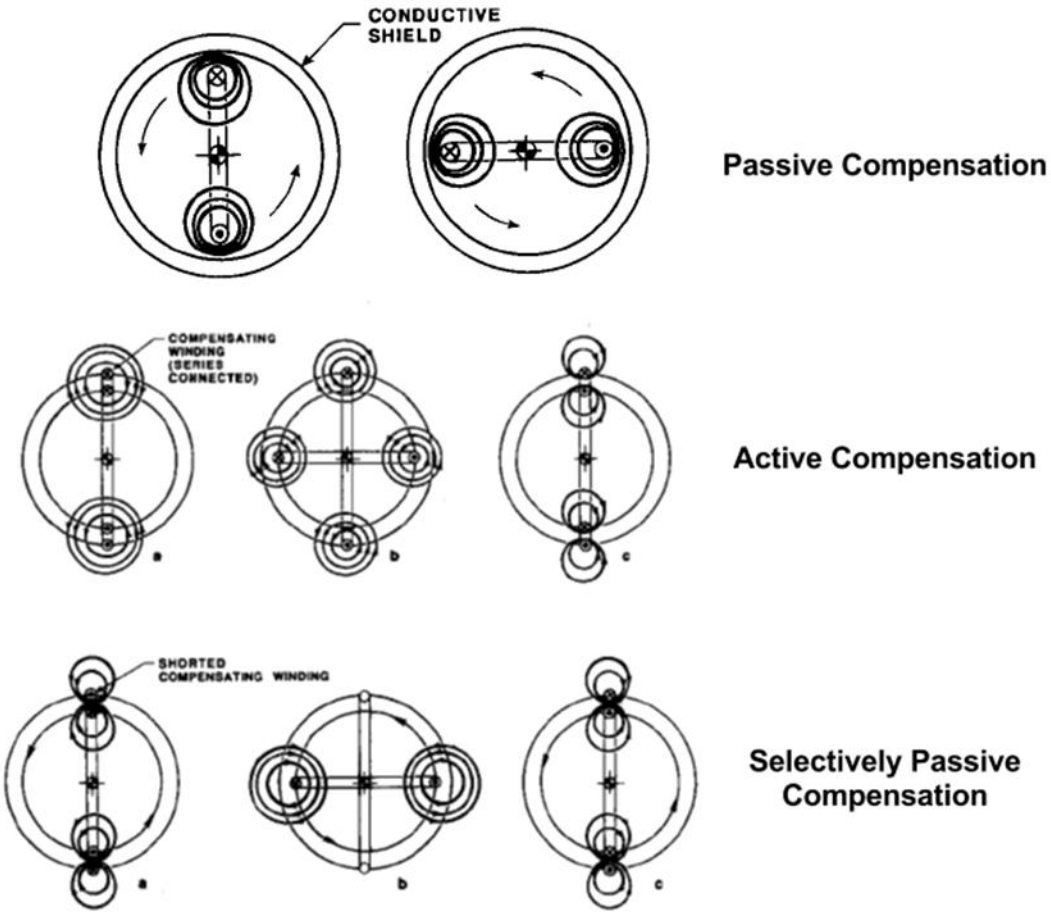

Figure 2: Different Compensation Schemes in Compulsators [4]

1.2.3.4.1. Passive Compensation

Passive compensation occurs when the compensating currents are induced in response to the transient armature fields produced during discharge [4]. The simplest form of this machine involves the use of a continuous conductive shield. During discharge, equal and opposite currents are induced in the shield. Because the shield is continuous, compensation is provided equally in all rotor positions resulting in a constant low inductance. A passively compensated machine will generate pulses that are effectively sinusoidal in shape [4]. This type of compensation is typically used in compulsators with iron-core magnetic circuits because they are typically insensitive to the time constant of the excitation field circuit [10]. Air-core machines require rapid self-excitation to achieve reasonable efficiencies; a uniform

compensation shield is not a practical option for air-core machines due to the length of time required for the excitation flux to penetrate it [10].

1.2.3.4.2. Selectively Passive Compensation

Selectively passive compensation is where currents are induced but compensation is not provided equally in all rotor positions, which results in a square output pulse shape [4]. Selective passive compensation can be employed in several ways, including non-uniform shielding or the use of shorted compensating windings. Both methods result in an inductance that depends on rotor position [4]. However, the compensating current is never in phase with the armature current and the flux compression ratio is significantly lower than in active compensation. At the start of discharge, if the compensation windings are aligned correctly, then current induced in the compensation winding compresses the armature flux to provide a lower inductance value [10]. The compensating winding axis is positioned so that maximum generated voltage coincides with minimum machine inductance, allowing for rapid rise in the output current pulse [10]. As the rotor rotates, the windings become out of phase and the armature flux is no longer confined. The lack of confinement increases the internal inductance, limiting the peak current achieved in the output pulse, and creates a flat pulse shape that is optimal for a railgun load [10]. As the rotor continues to rotate, similar interaction occurs that rapidly brings the current to zero [10].

The frequency of the induction variation is twice that of the machine electrical frequency [4]. This compensation scheme is extremely difficult to analyze since there are many variables related to the type of compensating winding, the orientation of the winding with respect to the excitation field, and the phase angle with respect to the open circuit voltage where the pulse is initiated [4].

1.2.3.4.3. Active Compensations

Active compensation occurs by connecting a second winding in series with the armature. In active compensation, the compensating current is forced to flow in a defined sense [4]. When the armature and compensating poles are aligned and the currents are 180 degrees out of phase, a low

inductance (roughly equivalent to the passive case) occurs. Meanwhile, when the rotor moves into a position where the two currents are in phase, a high inductance results. This variation of inductance is sinusoidal in nature, and high compression ratios of the maximum inductance to the minimum inductance occur [10, 4]. The active machine generates a narrow pulse of very high peak power.

1.2.3.5. Armature and Excitation Field Rotation Schemes

The relative velocity between the excitation field and the armature windings directly affects the voltage output of an electromechanical machine. Higher rotational velocities result in higher voltages as and also result in more inertial energy stored within the machine. However, there are practical velocity limits on systems with rotating elements that are typically defined by material property constraints.

Either a rotating armature or a rotating excitation field is chosen as the means of providing angular velocity between the excitation field and armature windings. Deciding between these two options is largely driven by structural requirements which are based on the energy delivery requirements of a system. A rotating armature is a system where the windings that are meant to interact with the magnetic field rotate during the operation of the compulsator, and the brushes that transfer the power are held stationary. A rotating field means that the windings or permanent magnets that generate the magnetic field are rotated while the armature windings remain stationary. In a rotating field configuration, the brushes rotate during the operation of the compulsator. There are different benefits and drawbacks to each option that must be considered [4, 10, 3].

1.2.3.6. Compulsator Excitation Schemes

For any electromechanical machine, a magnetic field must exist to interact with armature windings in order to generate voltage within the machine. Excitation generates the magnetic field within the compulsator, and can be accomplished through several different methods: permanent magnets, external excitation, and self-excitation.

1.2.3.6.1. External Excitation

External excitation is where powerful windings are run through the compulsator structure and a specified amount of current is carried through them similar to electromagnet operation. This excitation current generates a set magnetic field strength density within the compulsator for the armature windings to interact with. External excitation is a popular and relatively simple scheme used on a wide range of compulsator systems. External excitation was used on the first compulsator systems [4, 12]. There are significant design issues that must be accounted for when utilizing external excitation. Ohmic heating effects must be taken into consideration as thermal constraints can limit the maximum current that can be run through the external windings, or some form of cooling must be integrated into the system. External excitation windings require a large power supply to maintain constant current during operation. Structural integrity must be accounted for in the windings to ensure that they are not damaged from magnetic torquing during both operation and discharge. External excitation is typically a popular option with iron-core machines, which have a higher magnetic permeability and do not require high excitation energies [3].

1.2.3.6.2. Self-Excitation

Self-excitation can be pursued on both iron-core and air-core machines. However, due to the lower permeability and relative efficiency of air-core compulsators, drastically higher excitation energies are required [3]. These higher energies pose a difficult problem in providing a constant excitation current within the excitation windings of a compulsator, which would further compound thermal and structural issues already faced with external excitation.

Instead of a constantly provided excitation current, self-excitation operates in a more transient manner. In this mode of operation, the prime mover drives the pulsed alternator to a designated rotational speed. Once the desired speed is reached, a field initiation capacitor system discharges into the excitation field windings. Meanwhile the armature winding is connected to the excitation windings through a rectifier. The armature windings are rated to carry a high discharge current, the induced

voltage across the armature windings interacts with the excitation windings to excite the field. This is a positive feedback process. The current of the exciting field rises rapidly. Once the current rises to the desired value, the rectifier stops and then the compulsator discharges into the load [13]. Self-excitation is the most technically complex excitation scheme to implement, but results in the highest magnetic field strength densities.

1.2.3.6.3. Permanent Magnet Excitation

Of the three different options, permanent magnet excitation is the most basic to understand and implement. Permanent magnets of a specified magnetic field strength density are placed inside the compulsator as a replacement to excitation windings [14]. Due to the inherent magnetic field that exists, an excitation scheme can be implemented into a compulsator system in a straightforward manner, see sections 2.1.3. and 2.2.2.1. Care must be taken to ensure that the magnets are kept within their thermal limits so demagnetization does not occur. However, because there are physical limits to the magnetic field density strength of permanent magnet materials, this excitation scheme is typically utilized in iron-core compulsators.

1.2.3.7. Energy Reclamation

After discharge, significant amounts of magnetic energy can remain within a railgun barrel. Compulsators can be configured to reclaim this leftover magnetic energy through another route of switching circuitry back into the compulsator, this capability is not technically feasible in capacitive systems. Inductive energy reclamation is a complex process, but can drastically improve the efficiency of a compulsator. Typically, air-core compulsators will implement energy reclamation as a means to improve the overall system efficiency [13] because the lower magnetic permeability in an air-core machine results in a lower efficiency than iron-core.

1.3. Switching and Power Delivery

To maximize the efficiency to a railgun system, switching systems are put in between the pulsed power supply and the railgun. These switching systems provide additional control and safety to the system as a whole by controlling its output discharge. The switching circuitry is responsible for transferring all of the output power over a tiny (ms to μs) timespan, and must be rated to handle a high peak load during that time. Therefore, careful consideration must be taken into account for the design of the switching circuitry in any pulsed power application.

For this project, two electrical engineering undergraduate students and an aerospace engineering graduate student focused specifically on the design of the switching circuitry. Several compulsator design parameters can affect the design: the electrical frequency, the phase voltage, the number of phases, and the total electrical action per discharge [10]. For self-excited machines, the switching circuitry also provides the energy required to start the self-excitation process.

Early compulsators [7] relied on ignitrons, effectively a mercury-filled spark gap, as switches. Ignitrons are very effective high current rectifiers that provide a very quick rise time. Ignitrons must be triggered with an initial high voltage pulse to turn the mercury inside the chamber to arc and thus allow for current to flow from the pulsed power supply to the load. However, ignitrons have fallen out of favor as both performance requirements and technology advances have led to almost all pulsed power systems relying on solid state converters like large diameter SCRs [10].

High power switching circuitry is very costly and has extensive lead times (20+ weeks) if a requested switch is not in stock. Additionally, damage can occur to these switching elements during operation and that must be taken into consideration when scoping out a switching system for a pulsed power application.

1.3.1. Ignitron Switching Circuit

Budget and safety were the primary driving factors in the selection of a switching circuitry system for this project. The new switching system will be used for both capacitive and mechanical pulsed power systems, in an effort to stretch budgets as far as possible and allow for leftover resources to be used on different systems. An undisclosed Orange County power company donated several National Electronics NL7218H-100 ignitrons to this project. Due to budgetary constraints and long lead times to acquire different switches, these ignitrons were selected as the switching circuitry for this project. These ignitrons allow for switching up to 15 kV and have peak currents of up to 100 kA, which will be able to handle all of the switching needs for EMRG Mk 1.1.

Significant effort was undertaken by several members of the team to develop the ignitron switching circuit and its associated triggering circuitry [15]. For proper operation, a 5 μS pulse with a minimum voltage rating of 1500V is required of the system. More detailed information regarding the triggering of the ignitron switching circuitry was covered by an electrical engineering student on the team [15]. Below in is a picture of the ignitron switching circuit system:

Figure 3: Ignitron Switching Circuit system with associated support equipment

2.0 Compulsator Design

2.1. Architecture Selection

The two main factors behind the design decisions for this project's compulsator architecture were cost and complexity. All other compulsator system developed typically have had large budgets, extensive fabrication and testing facilities, and knowledgeable personnel that are well versed in pulsed power. The overall budget for this project was approximately $10,000, and almost everyone involved in the project started off with zero prior knowledge of pulsed power systems or compulsators.

One of the advantages that has made it possible for CPPP to develop such low-cost pulsed power supplies and electromagnetic railguns has been the projectile size. Since the projectiles launched by the railgun are very small (1g), the overall amount of energy required to be stored in a power supply drastically smaller (45 kJ versus 100s of MJ) than traditional military-funded systems. This has reduced the overall system mass and cost in CPPP's projects.

2.1.1. System Scoping

During the initial planning for this project, scoping of the system performance led to trying to match the performance of the existing capacitive pulse forming network (PFN) at Cal Poly. The existing PFN Mk 1 stored 16kJ of electrical energy and could accelerate a 1g projectile to 450m/s. A design target of 45kJ stored mechanical energy at 5,000rpm was chosen after extensive discussion between the author, the mechanical engineering students working on the project, and the designer of EMRG Mk 1.0. These values were selected to provide large factors of safety on rotating components and to account for low efficiency values.

2.1.2. Compulsator Topology Selection

Similar to Figure 1, a filled out compulsator architecture decision tree has been filled in to quickly visualize the topology of the Cal Poly Compulsator. This is seen below in Figure 4.

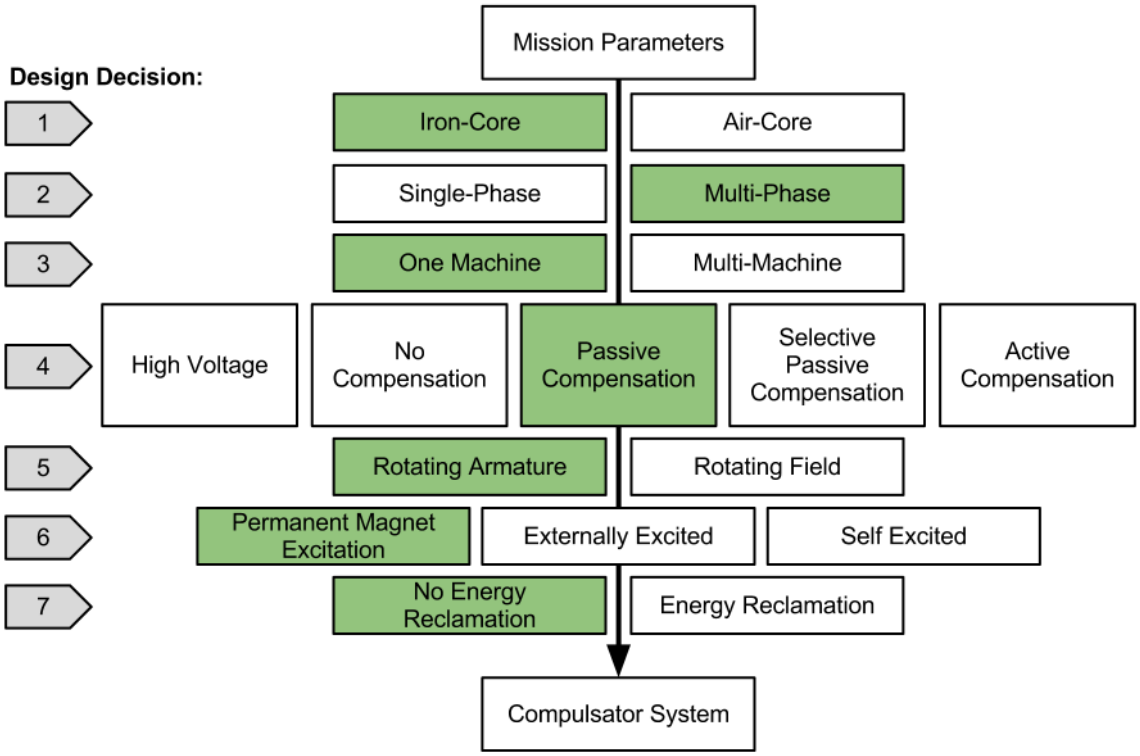

Figure 4: Cal Poly Compulsator Topology Selection Tree, the green highlighted sections represent the final architecture for the system

An iron-core, internal rotor, external stator topology was selected after examining the other options available. Air-core designs were discarded early due to the complexities involved in working with composite materials and their associated costs. Since this compulsator would only be rotating at 5,000 rpm it was decided that the system would have an external stator with an internal rotor, similar to a synchronous generator and most iron-core compulsators. Other compulsator systems that require very high operating speeds (10,000rpm and higher) are both typically air-core topologies and have an external rotor with an internal stator.

Below, in Figure 5 is a view of the Cal Poly Compulsator's external stator assembly and its internal iron-core rotor. These pictures were taken during the manufacturing and assembly stage of the project.

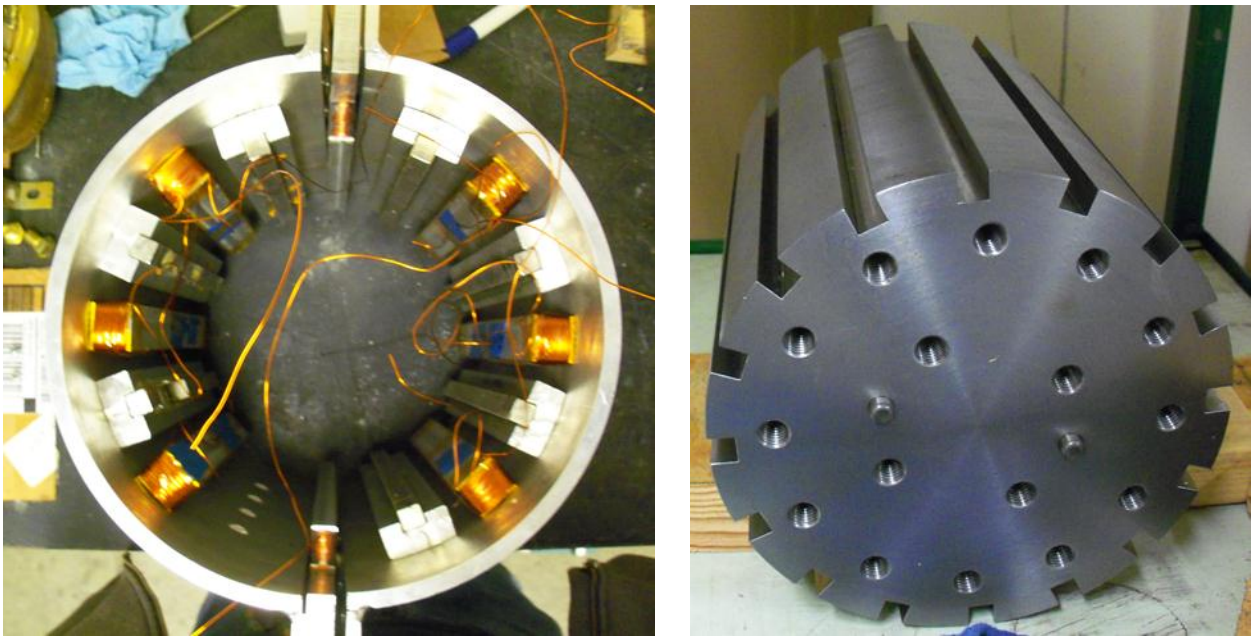

Figure 5: Compulsator Stator (Left) and Rotor (Right) Views, note the armature windings have not been included on the rotor yet.

2.1.3. Compulsator Excitation Scheme Selection

Internal-excitation schemes were discarded as well after an iron-core topology was chosen. Additionally, the complexity of internal excitation and its subsequent requirement for additional expensive switching circuitry to implement would have led to this scheme not being chosen. Furthermore, a lot of the mathematical analysis necessary to model this excitation scheme was above both the team's and author's capabilities.

Once internal excitation was ruled out, the selection of a prime mover was necessary. The prime mover's requirement would be to get the rotor up to 5,000 rpm within in a reasonable ramp up time over the course of several minutes. Then, the rotor would need to be decoupled prior to discharge. An electromagnetic clutch rated for the torque that would be seen at 5,000 rpm was selected to decouple the prime mover from the rotor shaft. By included a clutch, the need for designing a gearbox that would be have to go from 5,000 rpm to hundreds of rpm within milliseconds was avoided.

Next, the team explored the option of running current through the field windings on the stator for external excitation. The plan would have excitation windings providing the magnetic field that the copper windings on the rotor would rotate through, generating the electromagnetic field in the system. However, to create the magnetic field strength densities that the team was originally looking for at an original design goal of 1.25 Tesla this option became unfeasible. A power supply rated for nearly 10kW would have been required to generate the necessary magnetic field density; these power supplies typically cost thousands of dollars would have required too much of the budget for the project. Additionally, the steady state heating generated by the external field windings would have induced a variety of thermal heating problems into the system's design.

Finally, the team realized that permanent magnets could be employed for generating the necessary magnetic field density in the stator. Permanent magnets avoided the need for an expensive power supply and eliminate another set of windings in the system. One issue with permanent magnets is the cost of acquiring permanent magnets at field densities of up to 1-1.5 Tesla, and at custom sizes. After examining different options, Neodymium-Born permanent magnets were chosen for their high magnetic field strength density.

The associated costs of having custom-ordered Neodymium-Boron magnets were outside the budget for the project. Instead, a separate commercial vendor[1] of these magnets was found and individual .5inx.5inx.5in magnets were ordered. Because of this, an associated loss in magnetic field strength density occurred; these magnets only had a magnetic field strength of .45 Tesla. Furthermore, these magnets would have to be arranged into a line, with their magnetic poles aligned correctly into non-ferrous rails. This design decision resulted in assembly delays as a ferrous jig had to be manufactured to work with these smaller magnets. The magnets and the rails must be epoxied in place

[1] Permanent Magnet Vendor http://www.rare-earth-magnets.com/p-27-nsn0607.aspx

to prevent the magnets and/or magnet rails from shearing and contacting the rotor during discharge from magnetic forces. A picture of the completed magnet rail with the epoxied permanent magnets inside the channel can be seen in Figure 17.

Experimental results using this excitation scheme will determine how viable this excitation scheme will be. There are other permanent magnet compulsators in development [14] that have been tested as well, which helped to validate this design decision.

2.1.4. Compensation Scheme Selection

The compensation scheme selection for this project was a fairly straightforward process. Active compensation windings were too technically complex to attempt for several reasons. The winding topologies for active compensation are minimally documented, and the facilities to fabricate these windings were not accessible to the team. Similar reasons as those listed above ruled out selectively-passive compensation as well. This left the team with the only option of passive compensation. Luckily, the relative simplicity and comparative ease of integrating the aluminum compensation shield [16] [17] made this an attractive design decision. To provide passive compensation, a 1/16-inch thick aluminum sheet will be wrapped around the rotor and will be attached using epoxy on top of the rotor windings.

Another set of windings that was incorporated into the design are interpole windings located in-between the permanent magnet rails in the stator. The interpole windings were put in place to prevent the electric neutral plane from shifting during discharge [16]. Neutral plane shifts can occur due to armature reaction between the stator and the rotor, which can cause sparking and significant performance losses in the machine.

2.1.5. Rotor Winding Scheme

Copper windings within the rotor windings are necessary to generate an electromagnetic field as they rotate through the magnetic field generated by the permanent magnets within the stator. As

discussed later on in section 3.1.2 the voltage generated within the machine relies on the following equation [12]:

$$\boldsymbol{V_o = N_p N_{cp} l_r B v_{tip}}$$

N_p is the number of poles in the rotor, N_{cp} is the number of surface conductors per pole on the rotor, l_r is the length of the rotor (m), B is the strength of the magnetic field (T), and v_{tip} is the tip speed of the rotor (m/s).

Minimizing resistance is imperative to provide the highest discharge current possible, however the cost of materials and simplifying the winding scheme for future integration must be taken into account. Most compulsators use Litz wire for windings, which is a special type of magnet wire that is tightly bundled in a manner that minimizes the inductance of the windings. Unfortunately, Litz wire is an extremely expensive commodity and can only be ordered in minimum lengths of 1,000 feet. At the initial design phases of the project, not enough inherent knowledge had been built up by the author to even properly order Litz wire that would have led to proper performance goals. This combination of factors led to Litz wire being thrown out for rotor windings.

At this point in the design stage, the only parameter left available to increase the voltage was to increase the number of surface conductors per pole. Ideally, a large number of copper windings at the surface of each rotor slot to provide maximum possible voltage. In order to reach a voltage comparable to the 16 kJ 450 V capacitor bank that powers the EMRG Mk. 1, about nine conductors are required on the surface of each phase winding based on the already determined parameters: a rotational speed of 5000 rpm, rotor length of 10 inches, the number of poles being 8, and the magnetic field strength of approximately .45 T.

Since Litz wire was too expensive of a design option, insulated 10 AWG copper magnet wire was selected by the team for its relatively low resistance properties and bending capability for winding

construction. The decision to use 10 AWG copper magnet wire coupled with the geometric size of the permanent magnet poles limited the total number of surface conductor that can contribute to voltage generation. Because of this limitation, the original desired voltage of 450 V could not be met. The number of surface conductors is limited by the cross sectional length of the magnetic pole they are going to interact with as they rotate in the machine. A diagram depicting this issue is shown below in Figure 6:

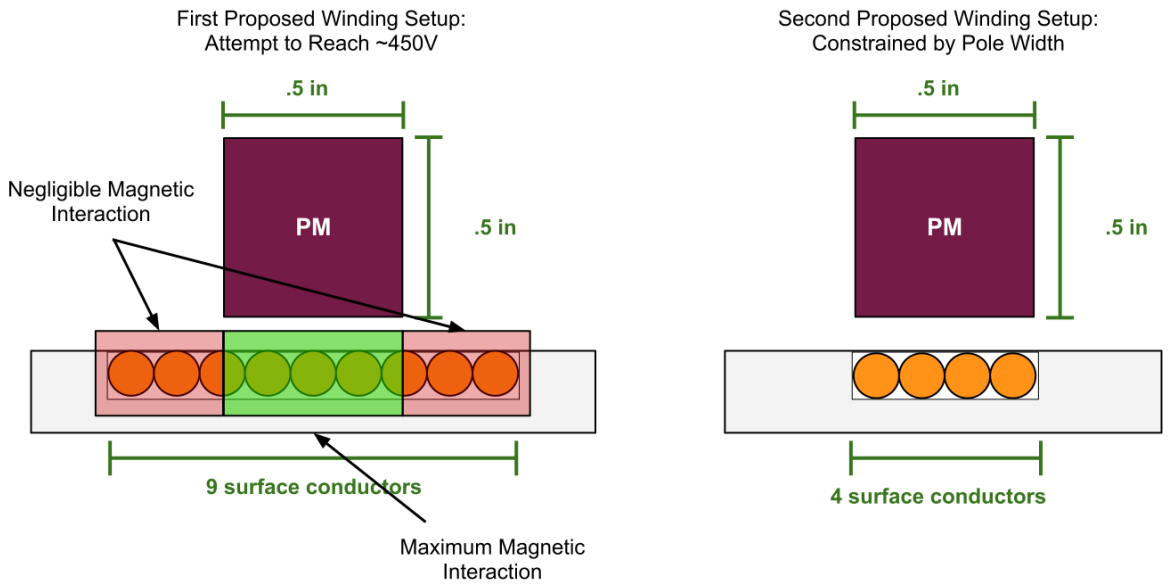

Figure 6: Rotor Phase Winding Interaction with Permanent Magnets

The number of surface conductors was then constrained to four since 10 AWG magnet was chosen for the armature windings. Smaller gauge wire would have higher resistance and negatively impact performance. Each phase winding is comprised of a single lap winding of wire with four turns, where each phase is separated by one rotor slot pair. Further detailed discussion on this winding is discussed in the following section. A diagram of these windings is shown below in Figure 7:

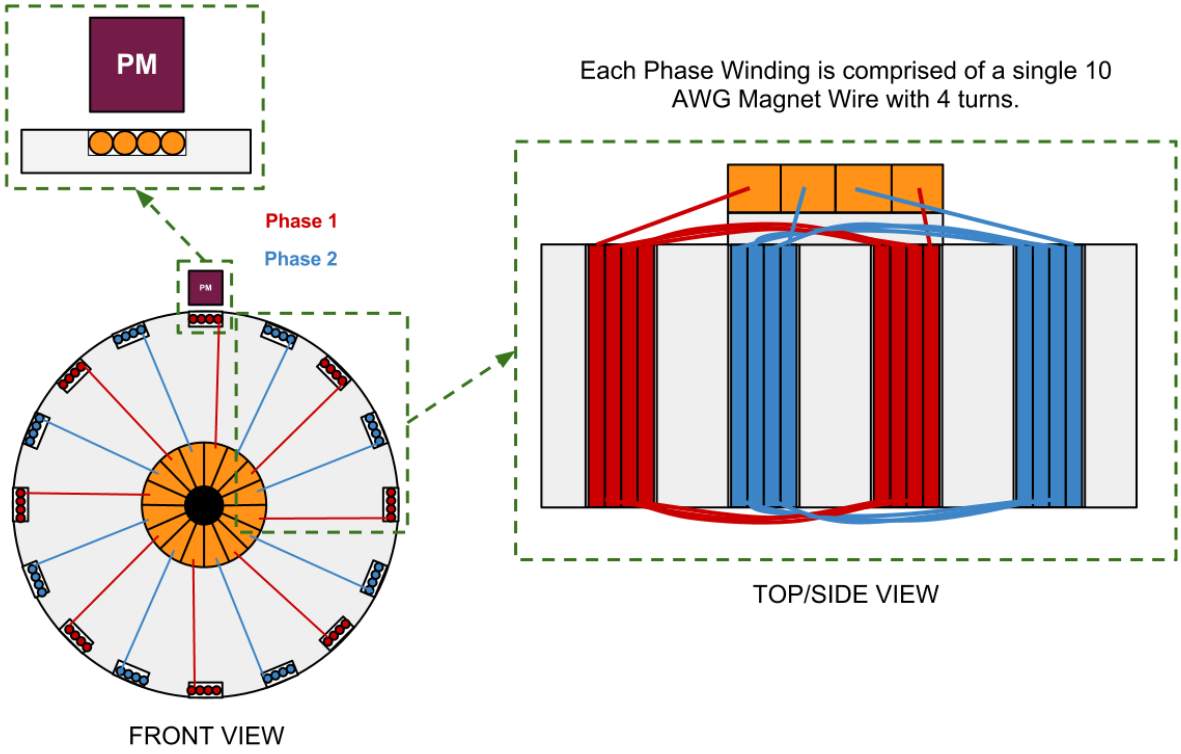

Figure 7: Schematic for the second proposed lap winding scheme.

Discussed later on in section 3.2.2 of the paper, it was found that compulsator discharge performance greatly falls off in the single-digit milliohm range. The proposed winding scheme above was found to have a resistance of approximately .0015 Ω, which had a predicted projectile performance of only 127 m/s. This loss in performance would not result in a system that would be comparable with the original 16 kJ capacitor bank that the team was looking to compare projectile performance to. Fortunately, this issue was found before any machining had occurred on the steel rotor section so a variety of solutions were available. In order to lower the resistance, the following options were considered:

- Increasing the gauge of the wire
- Less surface conductors (lowering the length of wire)
- Parallel paths inside the rotor slots

Option three, parallel paths, resulted in a solution that led to a lower resistance that also kept the number of parallel conductors still at four. The rotor slots were designed to go deeper than originally planned, by having four parallel windings of four turns stacked horizontally inside each rotor slot. Stacking the windings horizontally allowed for four separate surface conductors to interact with the permanent magnets. Additionally, having each of the windings in parallel and then brazed at the commutator lowers the resistance by a factor of four from the previous winding scheme. Instead of a resistance of .0015 Ω, a resistance of .000375 Ω was calculated, resulting in a calculated projectile performance velocity slightly greater than 400 m/s. A circuit diagram comparing the old winding scheme to the parallel path winding scheme is shown below in Figure 8

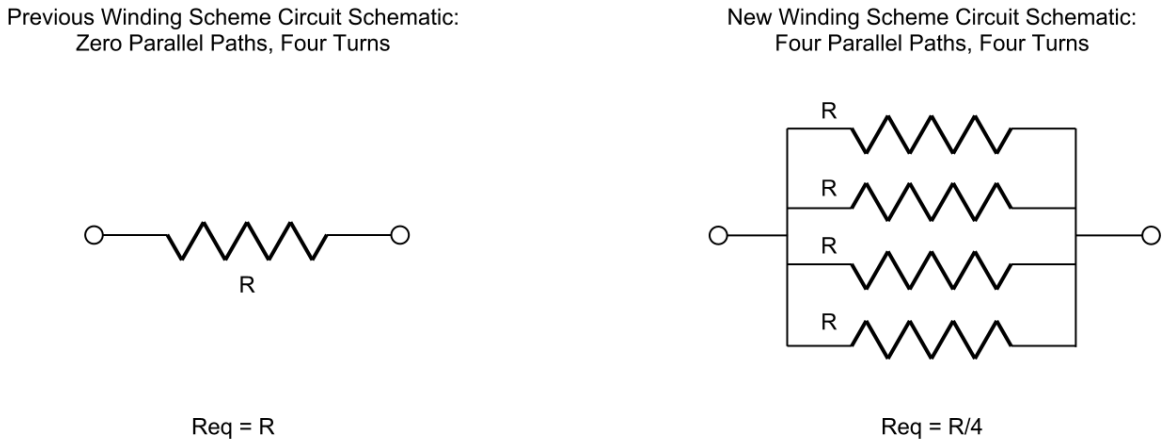

Figure 8: Circuit diagram examination of the previous winding scheme and the finalized design winding scheme with parallel paths.

The equivalent circuit diagram of four parallel paths, results in a complex but feasible winding scheme. This duplex lap winding scheme can be visualized in Figure 9 below. Each of the sixteen commutator pads would have four brazed connections to connect the parallel paths to the commutator. Each connection is one segment from each parallel path, while the turns for each path wrap to connect between their two corresponding slots. This is shown in the Figure 9 on the right side.

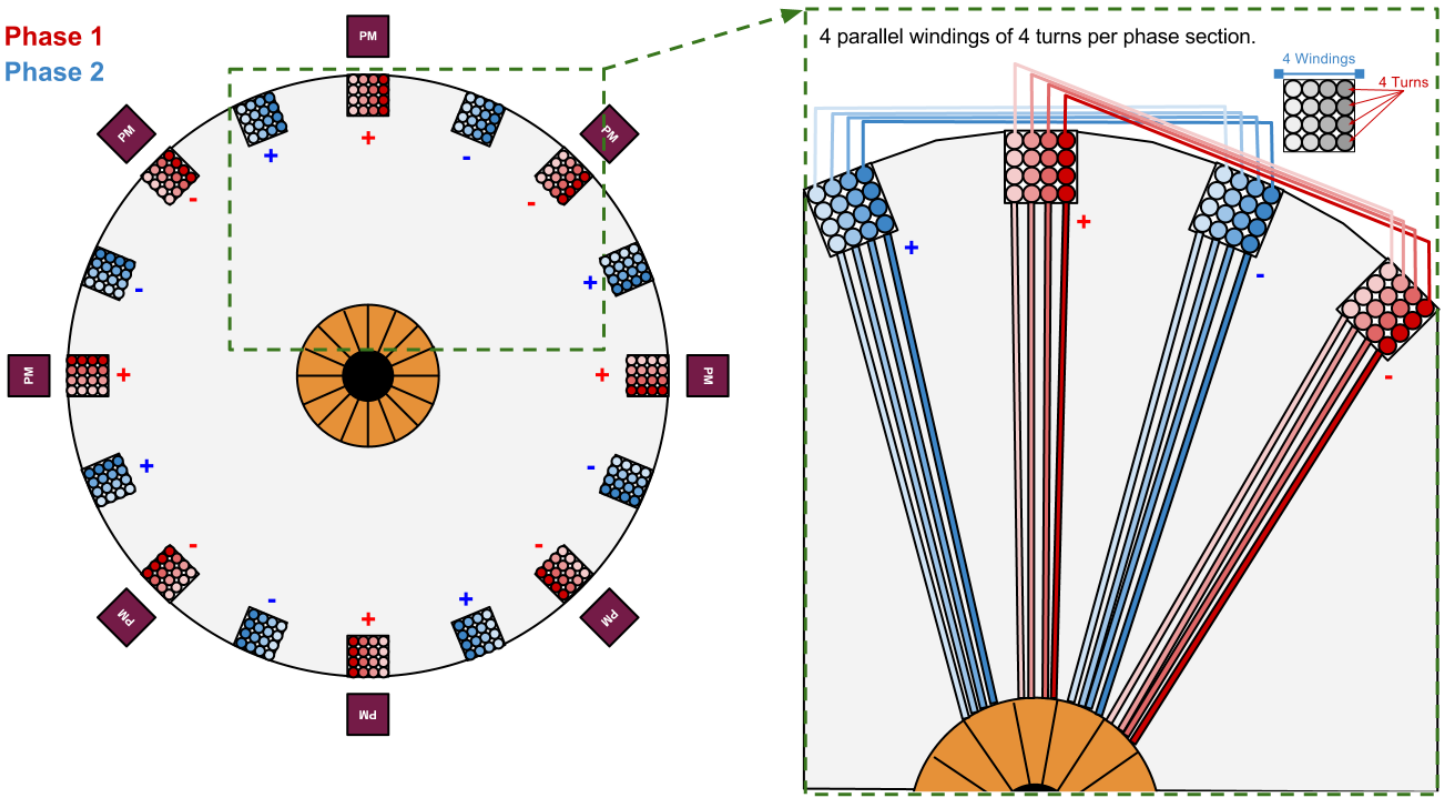

Figure 9: Lap winding scheme for two phases, with each phase having four parallel paths with four turns per path. Each unique parallel path is color coded for clarity.

Commutation is critical for both delivering the energy from the compulsator into the switching circuitry as well as rectifying the output to prevent the voltage from dropping below zero during operation. Ignitrons stop switching current if the voltage drops close to zero. By having two phases in the rotor with commutated outputs, the operational voltage never approaches cutoff. Based off of information gleaned from other papers covering this topic, a four phase system would have been the preferred choice. However, the winding scheme would have been even more complicated to implement on the rotor section and then braze to the commutator. Since a two-phase system met the discharge voltage requirements of the ignitrons, this became the final architecture decision for compulsator topology. A schematic detailing the voltage variation in each of the two phases during the rotation of the rotor is shown below in Figure 10:

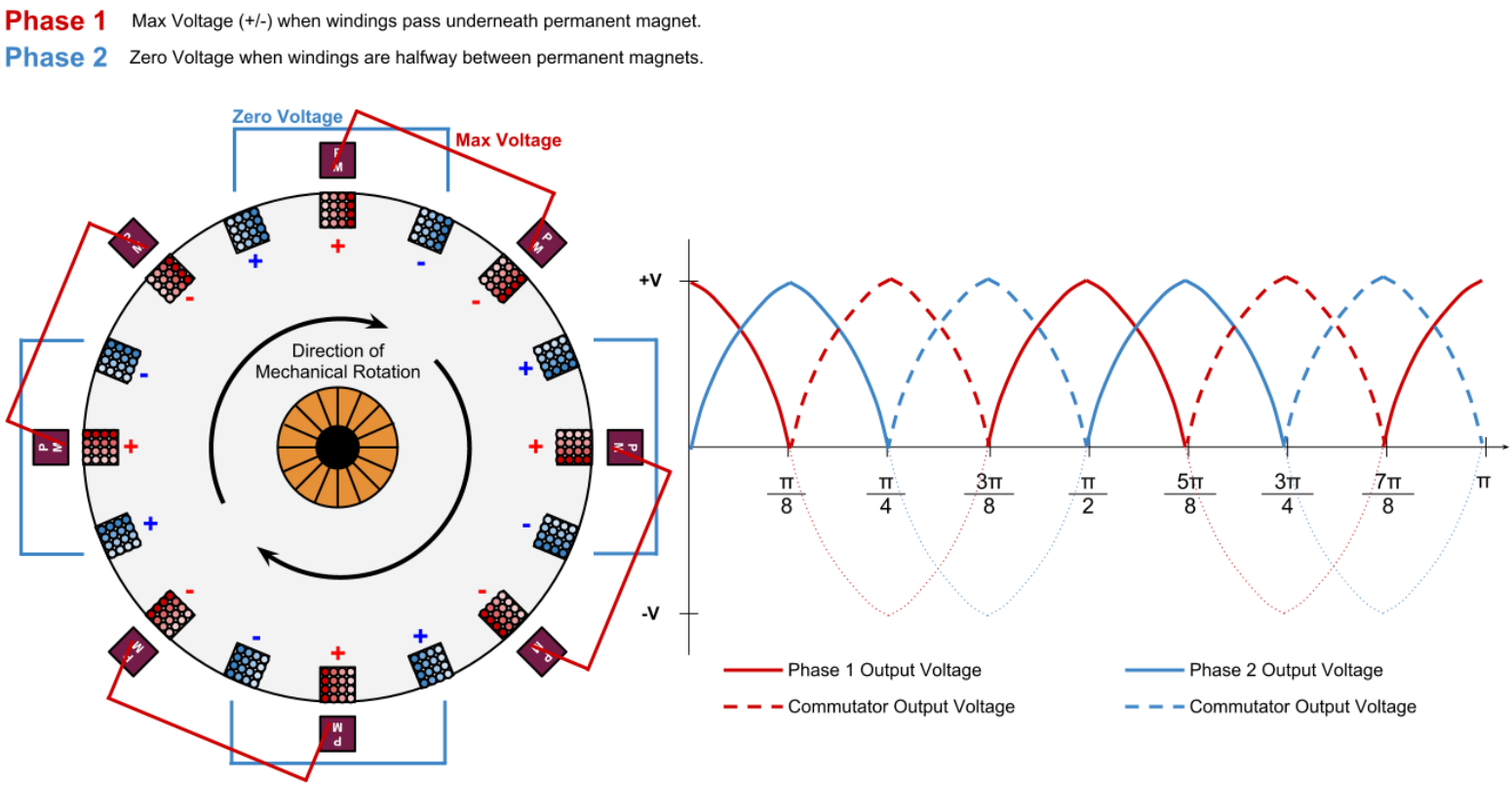

Figure 10: Output voltage relationship for each of the phases within the rotor, as well as the commutated output of both phases.

2.2. Finalized Compulsator Design

Section 2.1. covered the engineering process that led to the final design for the compulsator that is now currently undergoing fabrication and assembly. This section will go into further detail about the finalized design, as well as some of the fabrication processes that have already been completed. At the time of this publication, the system is still several months from final assembly and testing. A complete discussion of the remaining assembly, testing, and results analysis will be covered in the author's thesis. Significant discussion regarding the design is also covered in the report authored by the mechanical engineering students on the team. [17]

2.2.1. External Mechanical Systems

There are several mechanical systems on the outside of the compulsator that are responsible for ensuring successful operation of the machine throughout discharge. Detailed description of each system is included below, for reference a diagram of the external mechanical systems can be seen in Figure 11:

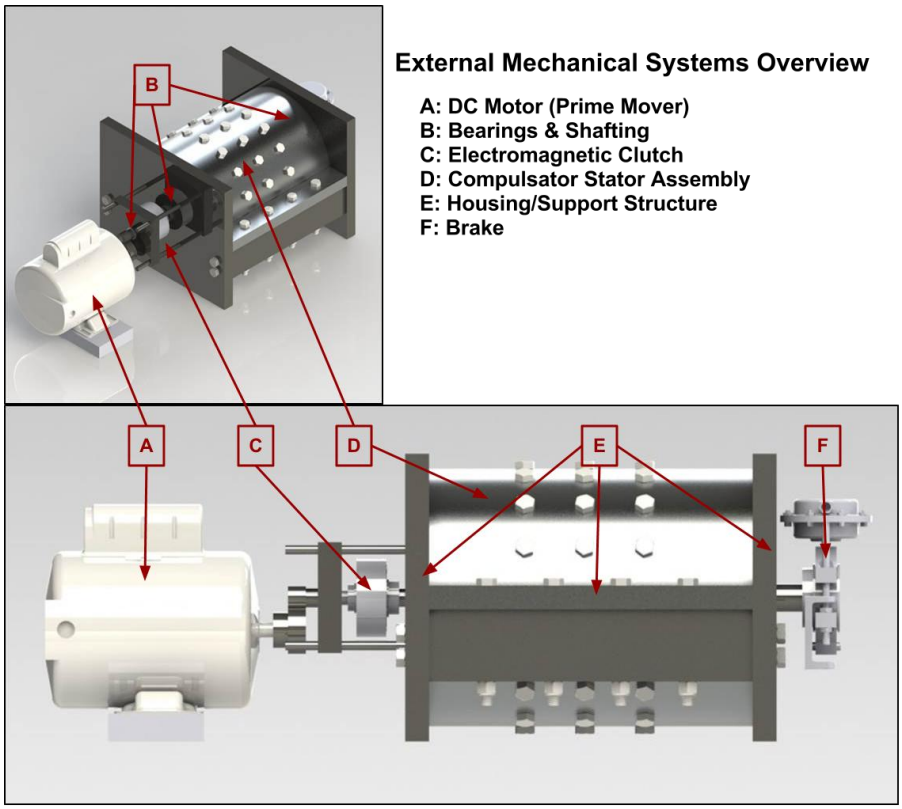

Figure 11: External Mechanical System Overview of the Cal Poly Compulsator

2.2.1.1. Prime Mover

The purpose of the prime mover is to provide the input torque necessary to get the rotor up to its operational speed of 5000 rpm. The prime mover creates the stored mechanical energy in the rotor and provides the relative angular velocity that generates the electromagnetic field between the rotor and stator assemblies. Taking into consideration ease of use and cost efficiency, a single-phase AC motor was selected. A one-horsepower motor was deemed sufficient to bring the rotor section up to speed in a reasonable time of approximately two minutes. [17]

Selecting a smaller prime mover had the added benefit of reducing overdesign on the gearing and shafting. The prime mover chosen is the McMaster (P/N 5990K23). This motor only had an operational speed of 1725 rpm, so a gear set was needed to reach the design speed of 5000 rpm. Analysis into the required gear ratios to reach 5000 rpm led to the decision of the following gear and pinion from McMaster (P/N 5172T24) & (P/N 5172T21). These gears are rated for ten hours of operation, have a projected lifetime of about 300 discharge events, and can be easily replaced [17].

2.2.1.2. Bearings and Shafting

The shafts used in the system are meant to allow for torque to be delivered from the prime mover into the rotor as well as provide rotational support for the moving components within the system. To handle these tasks, the shafting was broken up into three separate sections [17]:

- Pinion Shaft
- Clutch Shaft
- Brake Shaft

The pinion shaft contains the gears that rotate the system. It connects between a single bearing that is embedded in a small steel plate and one side of the clutch. The design constraints on the pinion shaft were the applied loads on the shaft due to the gear forces. The clutch shaft is the connection between the clutch and the rotor flange with a bearing support embedded within one of the two large

steel end plates of the support structure. It connects between the other side of the clutch and one end of the rotor. Lastly, the brake shaft connects between the brake and the other end of the rotor with a bearing support on the second large steel plate of the support structure. The de [1]sign constraint for these two shafts was to ensure that they could support the torsion load from shaft inertia during compulsator discharge. The braking torque was much smaller than the discharge-induced inertial torque, and did not constrain the design [17]. Calculations covering the various failure modes and analyzing for safety factors were handled by the mechanical engineering students on the project [17]. A view of the three different shafts is shown below in Figure 12:

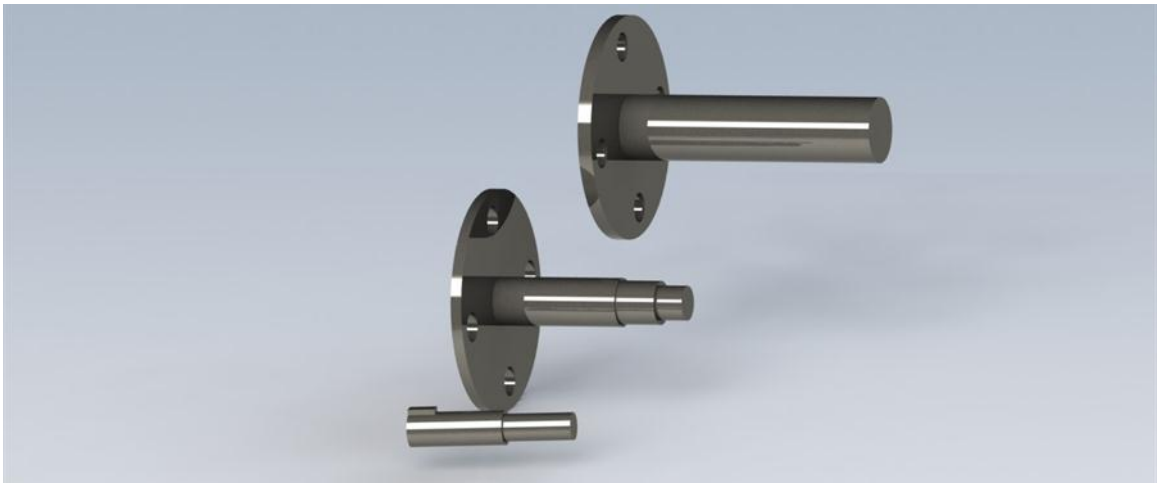

Figure 12: Shafting (from top to bottom) Braking Shaft, Clutch Shaft, and Pinion Shaft [17]

2.2.1.3. Electromagnetic Clutch

During discharge, the rotor will decelerate from 5000 rpm to below 200 rpm over a few milliseconds. This drastic reduction in speed would cause considerable damage to the existing gear assemblies, the prime mover, and the entire system. To prevent this damage from happening, some means of decoupling the prime mover from the rotor is required, and it was determined that a clutch be able to perform this critical task.

Two important factors were taken into consideration during the selection of a clutch. First, the inertial properties must be small enough to prevent the shafting from increasing in diameter. Secondly,

the clutch would need to handle the torque that would be seen during startup and operation. This led to the selection of a clutch from SDP-SI (P/N S90CSC-30A1010). It is designed for two inline shafts with a maximum operating speed greater than 5000 rpm and is capable of holding a torque of 125 in-lbs, while only 25 in-lbs will be seen on the clutch during startup [17].

2.2.1.4. Compulsator Stator Assembly

The purpose of the stator assembly is to house the rotor assembly and provide mounting surfaces for the stator's internal components that generate and support the magnetic field: the permanent magnet poles and the interpoles. One important factor in the design of the stator assembly was the capability to inspect, maintain, and repair the internal elements. In order to meet these capabilities, a modular stator assembly was designed. An added benefit to this modular approach is that future engineering students at Cal Poly can incorporate improvements to the system as part of their projects.

The stator is made up of two 6061 Aluminum semicircular sections. Bolt holes were cut throughout the circumference to allow for the internal components to be mounted to the interior of the stator. Further discussion on the internal components of the stator assembly (the permanent magnet rails and interpoles) will be covered in sections 2.2.2.1. and 2.2.2.2. respectively. A view of the stator can be seen in the figure below:

Number	Part	Material
1	Magnet Rail	6061 Aluminum
2	Interpole	6061 Aluminum
3	Epoxy	Epon 815C
4	Flange Weld	ER4043 Al Rod
5	Rail Bolts	6061 Aluminum

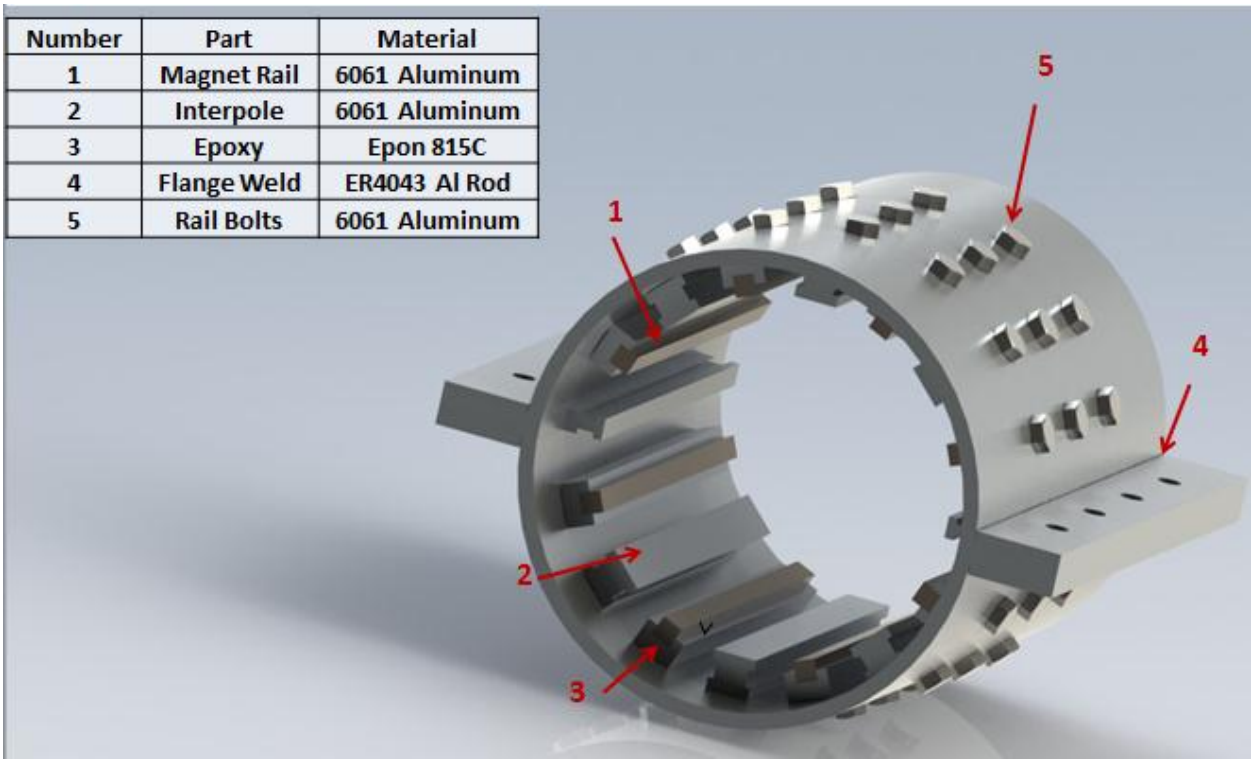

Figure 13: Stator assembly material type breakdown

Both the interpoles and the permanent magnet rails required additional structural analysis to ensure these elements would not be damaged by magnetic forces during discharge [17].

2.2.1.5. Housing/Support Structure & Foundation

The primary purpose of the housing and support structure is to provide the structural support for the compulsator and house internal systems. The design of this system was fairly straightforward. Two large 12'' x 14'' x 1'' 1018 low carbon steel plates were selected for the end plates. These plates would provide the primary structural support for the compulsator and allow for bearings to be placed through them to support the rotor.

The other support structures were two 2'' x 3'' x 13.5'' A36 hot rolled steel bars. These connect the two end plates and below the stator assembly bolt connections. Pictures of these structural elements can be seen in Figure 14 and Figure 15 below.

Figure 14: Compulsator Supporting Structure Steel Housing Rails

The housing rails support the stator assembly and drive loads into the end plates down into the concrete base below the compulsator.

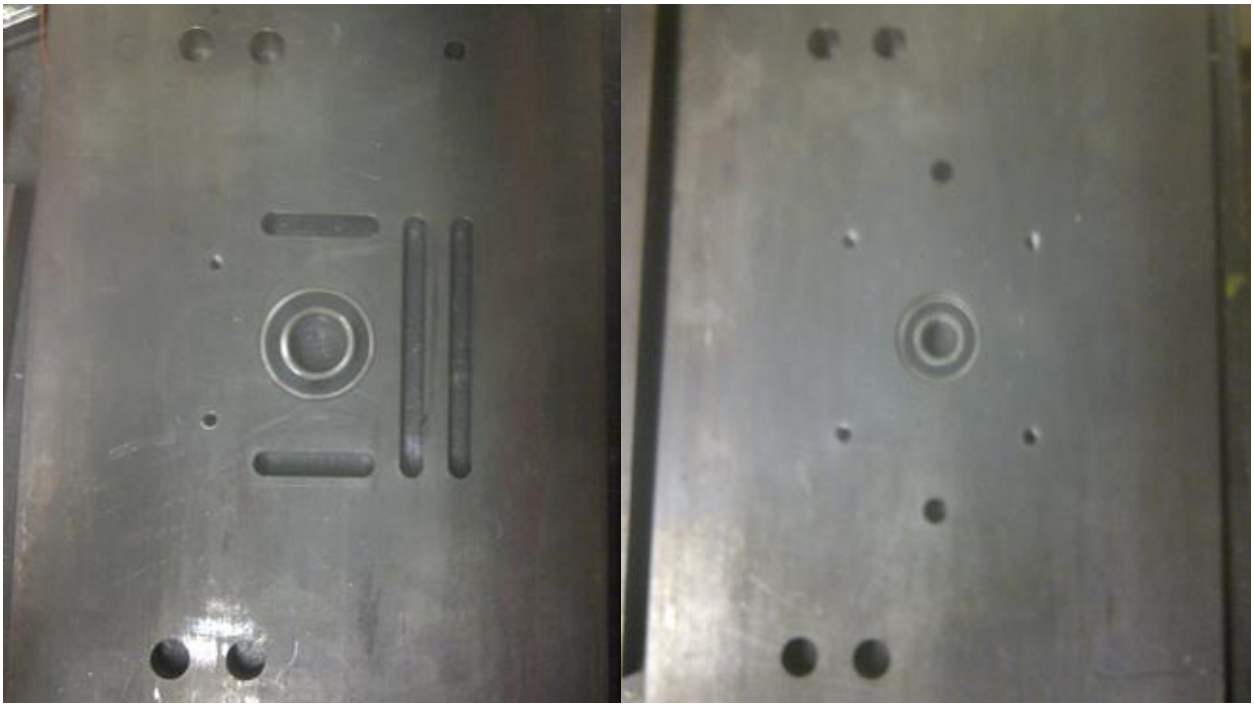

Figure 15: Picture of the completed end plates. Left: Brake shaft end plate, Right: Commutator side end plate.

The end plates provide the primary support for the compulsator; these are anchored to a large concrete base foundation. The concrete base is meant to absorb vibrations induced by the rotating machinery of the compulsator, as well as to simplify transportation of the system. The base is a 4'x4'x1' concrete section surrounded by a wooden frame with slots underneath for forklift-capable transportation. A picture of the concrete base is shown in Figure 16.

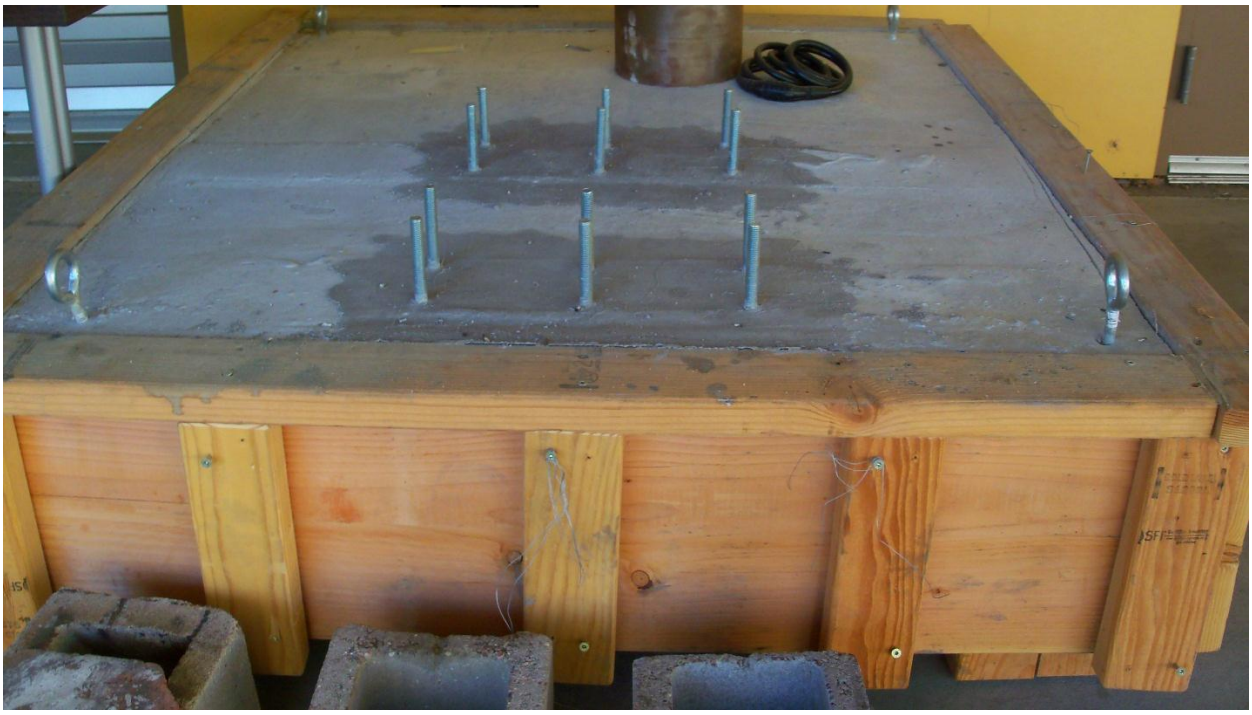

Figure 16: Compulsator concrete base, approximate weight 1,500-2,000 lbs.

2.2.1.6. Brake

The brake connects to the brake shaft, and the brake performs two separate functions during operation. First, the brake is meant to serve as an emergency safety device for the duration of operation. If there are any critical issues that jeopardize the safety of any personnel in the testing area, then the brake will be engaged to abruptly stop operation of the machine. Calculations undertaken [17] showed that the brake would stop rotation from 5000 rpm to zero over five seconds.

Second, the brake is also meant to be engaged after a discharge event to stop the rotor's residual rotational energy leftover after firing. The selected brake was a frictional brake from Nexen (P/N J 841600), (P/N 842100), (P/N 842000). The selected brake is an air brake and requires a compressed air supply for operation in order to clamp down pads on the drum brake attached to the shaft.

2.2.2. Internal Mechanical Systems

The following sections discuss the internal mechanisms of the compulsator, and their functional roles leading up to, during, and after the discharge event.

2.2.2.1. Permanent Magnet Poles

As discussed in the section 2.1.3., the team selected permanent magnets for the excitation scheme to generate the magnetic field in the stator assembly. To minimize cost, several hundred .5" x .5" x .5" Neodymium-Boron permanent magnet cubes were purchased from MAGCRAFT. The plan was to align the north and south faces of the magnets in a row along the length of the stator. In order to support the magnets, a 6061 Aluminum rail was designed for both holding the magnets in place and providing the necessary structural support to handle the magnetic forces seen during discharge. FEA and hand calculations were performed to ensure there was a wide factor of safety in the design [17]. These calculations were done originally for a magnetic field strength density of 1.25 Tesla, however the magnets purchased had an actual field strength density of approximately .45 Tesla. All structural elements within this machine were already designed to this field strength density, thus increasing all safety margins related to magnetically induced forces. Below are some pictures of what the finished magnet rail looks like with the magnets epoxied into the channel:

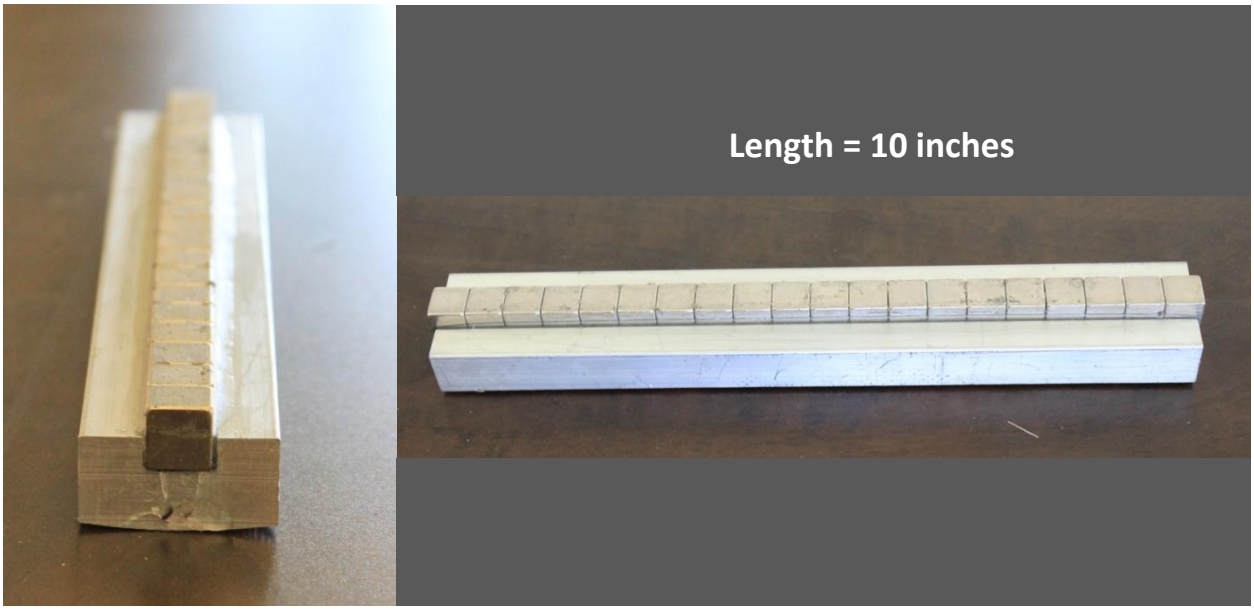

Figure 17: Close up view of the permanent magnet rails with magnets already inside

Eight of these rails were machined and filled with magnets. The magnets were analyzed and marked to designate the north and south faces [16]. Each rail comprised of 20 magnets all oriented in the same magnetic direction. There were a lot of integration and assembly issues that had to be overcome to reach the magnet configuration shown above. First, the permanent magnets posed a risk to any electronic devices near the work area, so all sensitive devices were cleared from where work would be handled on the magnets. Second, the magnets required 20-30 pounds of force to separate from each other and they frequently would come into contact with each other or other ferrous objects and tools in the work area. The simple solution for separating two magnets is to apply a shearing force and pulling to separate them easily.

Significant magnetic forces made the task of aligning and epoxying twenty .5” x .5” x .5” permanent magnets into an aluminum channel nontrivial. Overcoming this assembly problem was an interesting design challenge. The magnets were placed inside of a steel jig with a half-inch channel milled out for the magnets to be aligned within. Then the aluminum rail was coated in epoxy and

clamped onto the magnets in the channel. The epoxy would sit for 24 hours and the steel jig would be removed with a shear force, leaving the completed magnet rail ready for use.

2.2.2.2. Interpoles

The function of the interpoles is to realign the magnetic field between the rotor and stator during discharge. In electric machines there are planes where minimal magnetic fields exist, which are referred to as neutral planes. These locations are also best suited for brush location to prevent sparking due to the reaction between the discharge current and the magnetic field [16].

Based on calculations handled by one of the mechanical and electrical engineering students on the team, it was found that the interpoles would have 80 turns of 24 AWG insulated magnetic copper wire. Eight total interpoles were constructed. Six of them were constructed out of 6061 aluminum bars that had channels cut into the sides to allow room for the copper windings. Below is a view for the six regular interpoles:

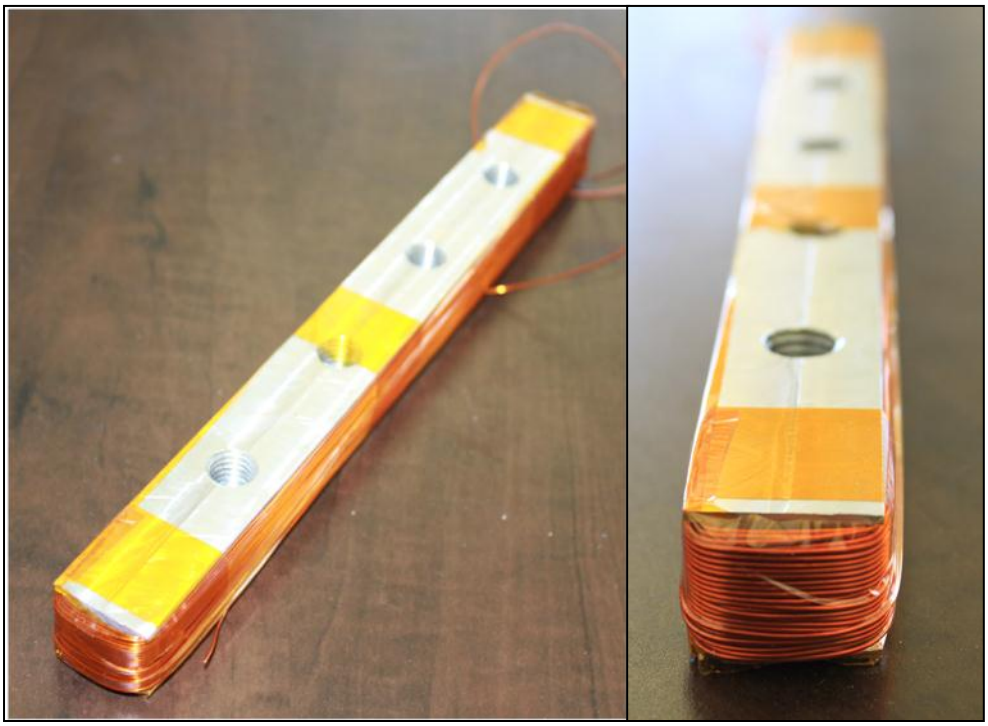

Figure 18: View of 1 of 6 regular interpole rails with copper windings already wrapped

The other type of interpole that had to be constructed was the flange interpoles, which were placed in between the two semicircular halves of the stator. An image of these rails can be seen in Figure 19:

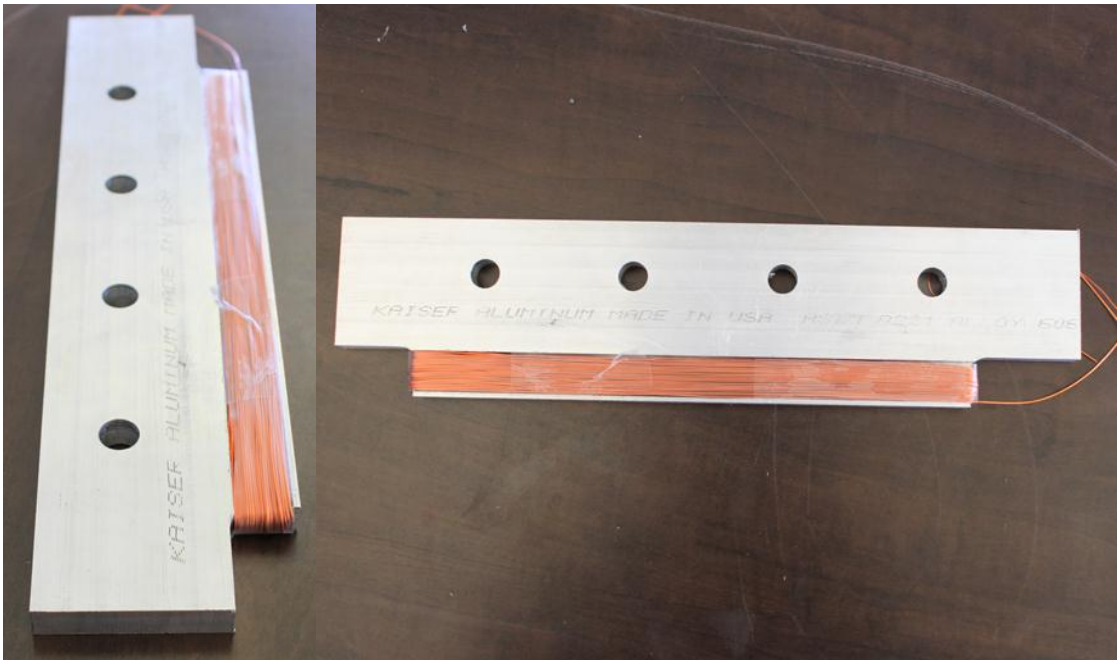

Figure 19: View of the 2 interpole flanges with copper windings already wrapped

These interpole flanges were sandwiched between the two stator sections, with bolts running through the holes. The interpoles were all wrapped in the same direction, so care must be taken to ensure that the wire leads coming off of each flange must be connected in a manner that will alternate the electromagnetic field direction generated by each interpole. These wire leads will be connected in parallel to the output of the compulsator. A resistor of a specified resistance is placed in between the interpole windings and the compulsator output. Connecting the interpole windings to the output allows for a dynamic response to the transient discharge environment and should passively be able to prevent a neutral plane shift from occurring [16].

2.2.2.3. Rotor Assembly

The rotor's purpose is to provide both the mechanical energy storage from its rotational inertia. Additionally, the rotor provides the slots for the copper armature windings that will interact with the poles in the stator to generate voltage in the system. A cylindrical section of 1018 cold rolled steel of 8-inch diameter and 10-inch length was purchased. After CAD work and follow-up structural design [17], the machining was contracted out to a fabrication facility off campus, Next Intent. Threaded holes were created on each side of the rotor to allow for follow up balancing to be performed on the rotor after final assembly is completed. An image of the completed rotor section can be seen in Figure 20:

Figure 20: Machined rotor section with rotor winding slots cut out as shown.

The rotor will have both shafts press-fit and screwed into each of the faces of the cylindrical rotor. [11]

2.2.2.4. Compensation Shield

In order to lower the inductance of the machine and help shape the discharge pulse, a passive scheme was selected. The passive compensation shield is a thin 1/16-inch sheet of aluminum that will be wrapped around the circumference of the completed rotor assembly. It will be epoxied into place and wrapped tightly to hold its form around the rotor assembly. Care must be taken to ensure that the surface finish will have minimal undulation so the small air gap in between the stator elements and the compensation shield can be maintained.

2.2.2.5. Commutator and Brush Assembly

The purpose of the commutator is to rectify the AC voltage output of the compulsator into a DC voltage. The DC voltage output is then fed to the switching circuitry and the railgun load, which requires a DC input for operation. The commutator used for this system was donated by Kirkwood Industries Toledo Commutator. The commutator received had 16 pads, where a total of 8 brushes would be used for the two-phase output. The commutator is rated for 1500 V and 16,000 RPM @ 350 ^{o}F.

The original brushes that were received to work with the commutator were graphite and measured .25x.375x1.0 inch. These brushes were found to have too high of a resistance, and a new solution had to be found. Copper bar segments of the same dimension were machined as a replacement for the graphite. These copper brushes have a much smaller resistance and will not impact the output performance of the compulsator. However, care must be taken to minimize any thermal effects and degradation to the commutator for having copper on copper rotational connections during operation. Inspecting the commutator for damage will be required before any series of test runs is occurs. To mitigate thermal effects a copper/graphite composite material will be purchased and machined to the same dimensions as a replacement brush material instead of pure copper brushes.

After the rotor windings are completed, the terminal connections that will attach to the commutator will be brazed onto the commutator. Each pad of the commutator will have four brazed

connections from the phase windings, enough clearance space open for the brushes to run across the commutator pads.

3.0 Compulsator Modeling, Analysis, and Results

3.1. System Modeling and Analysis

This section of the paper will cover the equations used in the modeling of the compulsator-railgun system. These equations were pulled from a variety of published sources, and have been compiled and organized for the benefit of anyone working within the pulsed power field. Significant effort was spent navigating between various published materials that led to the combined model of differential equations that will model the discharge of an iron-core compulsator.

Other useful papers were found that contained different analysis routes and governing equations for a variety of compulsator architectures. Due to differences in the physical architecture of the Cal Poly Compulsator, the analysis outlined in these papers was not used in section 3.1.1. However, references have been included to these papers since relevant information related to compulsator operation and design considerations are contained within these papers [18, 7, 19, 20, 21].

3.1.1. Railgun Governing Equations

Electromagnetic railguns impart acceleration upon their projectiles through the Lorentz Force and this force can be simplified to the following [11] :

$$\boldsymbol{F = j \times B = \frac{L' I}{2}} \tag{1}$$

F is the force on the railgun projectile, *j* is the current density (A/m^3), *B* is the magnetic field strength (T), L' is the inductance gradient of the rails (H/m), and I is the discharge current inside the railgun (A). Relating the force in equation 1 to Newton's second law, the acceleration of a particle inside a railgun can be found, seen in Equation 2:

$$\boldsymbol{\frac{d^2x}{dt^2} = \frac{L' I^2}{2m}} \tag{2}$$

The notation has been modified in terms of dx/dt where x is projectile position in the rails (m), dx is projectile velocity in the rails (m/s), and d2x is projectile acceleration in the rails (m/s2). Additionally, m is the projectile mass (kg). This change in notation is important because the modeling of the

compulsator-railgun system is converted into state-space form to combine the governing equations of these two systems. The velocity of the projectile within the railgun is found through numeric integration of Equation 2. For the analysis covered in this paper, that numeric integration was handled using the ode45 function in Matlab.

3.1.2. Supporting Compulsator Electromechanical Equations

The following equations are used to calculate a variety of parameters that must be known in order to model the interaction between the railgun and compulsator during discharge. The voltage within the compulsator will have a sinusoidal oscillation, which can be calculated using the instantaneous voltage equation for a rotating machine [22]:

$$\boldsymbol{V(t) = V_o\, sin(\omega_e t)} \tag{3}$$

V(t) is the instantaneous voltage at any given moment in time, V_o is the rotational emf voltage of the compulsator, ω_e is the electrical frequency of the compulsator (Hz), and *t* is time (s). The equation used to calculate V_o is the following [12]:

$$\boldsymbol{V_o = N_p N_{cp} l_r B v_{tip}} \tag{4}$$

N_p is the number of poles in the rotor, N_{cp} is the number of surface conductors per pole on the rotor, l_r is the length of the rotor (m), *B* is the strength of the magnetic field (T), and v_{tip} is the tip speed of the rotor (m/s). The other parameter from Equation 3 is the electrical frequency, which is calculated using the following equation [10]:

$$\boldsymbol{\omega_e = \frac{\omega_m N_{pairs}}{2\pi}} \tag{5}$$

N_{pairs} is the number of pole pairs in the compulsator, and ω is the mechanical angular velocity (rad/s). From Equation 4, rotor tip speed is found using the following expression:

$$\boldsymbol{v_{tip} = \frac{RPM\pi D_r}{60}} \tag{6}$$

RPM is the rotations per minute of the rotor; D_r is the diameter of the rotor (m). Another important parameter that needs to be known within the machine is the resistance within the rotor windings, which is approximated using the following equation [23]:

$$\boldsymbol{R_{ac} = \frac{l_{phase}\rho}{D\pi\delta}} \tag{7}$$

R_{ac} is the AC resistance (Ω) that accounts for the skin effect on the rotor windings, since the operation of the compulsator is AC. l_{phase} is the length of the windings for one phase (m), ρ is the resistivity (Ω/m), and δ is the skin depth (m). The skin depth is found with the following equation [23]:

$$\boldsymbol{\delta = 503\sqrt{\frac{\rho}{\omega_e \cdot 1}}} \tag{8}$$

The physical length of each phase winding in the rotor was approximated with the following calculation:

$$\boldsymbol{l_{phase} = N_t \cdot l_{turn} + l_{cmttr}} \tag{9}$$

N_t is the number of turns per phase, l_{turn} (m) is the length of the windings per turn, l_{cmttr} (m) is the length taken from the commutator to the windings.

3.1.3. Compulsator Governing Equations

The discharge current of a compulsator is found by examining the ratio of magnetic flux linkage over the inductance of the compulsator over time [24]:

$$\boldsymbol{i(t) = \frac{\Phi(t)}{L(t)}} \tag{10}$$

$i(t)$ is the discharge current (A), $\Phi(t)$ is the magnetic flux linkage (V·s), and $L(t)$ is the instantaneous inductance (H). Inductance plays a critical role in the performance of a compulsator, the instantaneous value for inductance during operation is found with the following equation [6, 22]:

$$\boldsymbol{L(t) = L_{min}\rho_c\, sin(\omega_e t - \delta_e)} \tag{11}$$

L_{min} is the minimum inductance of the compulsator, ρ_c is the compulsator inductance modulus, δ_e is the electrical phase angle (rad), and t is time. The compulsator inductance modulus is calculated with the following relationship [6]:

$$\boldsymbol{\rho_c = \frac{1}{2}\left(\frac{L_{max}}{L_{min}} - 1\right)} \tag{12}$$

L_{max} is the maximum inductance of the compulsator. The maximum and minimum inductance values were approximated by another student working on the project [16]. Calculating the magnetic flux linkage is a very difficult calculation to tackle directly. Instead, calculating the rate of change of current and the current can be found through numeric integration. Through the use of the following equation, the discharge current rate can be found with the following equation [6]:

$$\boldsymbol{\frac{dI}{dt} = \frac{V - I(R_c + R_o + R'x) + I\left(\omega_e L_{min}\rho_c \sin(\omega_e + \delta) - L'v_p\right)}{L_{min}(1 + \rho_c) + L + L'x + L_o}} \tag{13}$$

dI/dt is the discharge current rate of change (A/s), V is the compulsator voltage (V), I is the instantaneous current (A), R_c is the compulsator's internal resistance (Ω), R_o is the resistance of the connections from the compulsator to the railgun (Ω), R' is the resistance of the railgun (Ω), x is the particle position inside the railgun (m), L' is the inductance gradient of the railgun (H/m), v_p is the velocity of the projectile inside the railgun (m/s), and L_o is the inductance of the connections from the compulsator to the railgun (H). R_o and L_o should be kept close to R_c and L_{min} respectively to reduce losses within the system. The mechanical energy stored within the compulsator is simply calculated by the kinetic energy equation for a rotating object:

$$\boldsymbol{E = \frac{1}{2}J_r\omega_m{}^2} \tag{14}$$

E is the mechanical energy stored (J), J_r is the polar moment of inertia of the rotor(kg-m^2/rad^2). From this equation a relationship was found to approximate the change in rotational velocity during

discharge. This can be found in the following equation, a step-by-step of the equation manipulation and substitutions can be found in Appendix B: Energy Discharge Equation Derivation:

$$\frac{d\omega}{dt} = \frac{-\sqrt{\frac{2VI}{J_r}}dt}{dt} \tag{15}$$

3.1.4. State-Space Modeling of the Railgun-Compulsator System

From the equations outlined in the above sections, a state space model was developed that would rely on numerical integration to model the discharge of the compulsator.

$$\begin{bmatrix} u_1 = \omega \\ u_2 = x \\ u_3 = {dx}/{dt} \\ u_4 = I \end{bmatrix} \xrightarrow{\text{derivative}} \begin{bmatrix} du_1 = {d\omega}/{dt} \\ du_2 = {dx}/{dt} \\ du_3 = {d^2x}/{dt} \\ du_4 = {dI}/{dt} \end{bmatrix}$$

All of the equations from the above analyses were implemented into Matlab as a function that handled the calculations for modeling the discharge. The relevant Matlab files that handled this analysis are included in Appendix A: Matlab code of Compulsator Discharge.

3.2. Theoretical Analysis and Results

3.2.1. Cal Poly Compulsator System Parameters

The input parameters for this system are listed in Tables 1-3 below. For the benefit of the reader, an additional column is included to provide some context to how each variable's value was determined. Table 1 covers the physical parameters taken from the EMRG Mk. 1 railgun that the compulsator will use as its load.

Table 1: EMRG Mk. 1 Railgun Parameters

Variable	Value (units)	Method Determined
X_{rg}	.7620 (m)	Measured
R'	2.45e-04 (Ω/m)	Calculated
R_{rg}	3.21e-04 (Ω)	Measured [2]
L'	3.27e-07 (H/m)	Calculated [2]
m	.001 (kg)	Measured

Table 2 contains the parameters that were used in the discharge simulation for the compulsator system.

Table 2: Compulsator Input Parameters

Variable	Value (units)	Method Determined
N_p	8	Known
N_{pairs}	4	Known
N_{cp}	4	Known
B	.45 (T)	Measured
D_r	.2 (m)	Measured
L_r	.25 (m)	Measured
J_r	.334 (kg-m^{2}rad^{-2})	Calculated
L_{min}	1e-5 (H)	Approximated [16]
L_{max}	1e-5 (H)	Approximated [16]
R_c	3.75e-4 (Ω)	Calculated
R_o	1e-6 (Ω)	Assumed
L_o	1e-6 (H)	Assumed
$\delta_{e\ (phase\ 1)}$	0 (rad)	Known
$\delta_{e\ (phase\ 2)}$	π (rad)	Known

Table 3 lists the initial conditions of the compulsator just before the discharge event.

Table 3: Compulsator Initial Conditions

Variable	Value (units)	Method Determined
RPM_0	5000 (rpm)	Assumed
ω_0	524 (rad/s)	Calculated
V_0	194 (V)	Calculated
x_0	0 (m)	Assumed
v_{p0}	0 (m)	Assumed
I_0	0 (A)	Assumed

3.2.2. Discharge Performance Results from Theoretical State Space Model

The following pages include figures showing the calculated output performance of the compulsator during discharge. For reference, the following output performance parameters were calculated with the Matlab simulation using the analysis from the section 3.1.:

Table 4: Compulsator Discharge Performance Values

Variable	Value (units)	Method Determined
$V_{p,final}$	410 (m/s)	Calculated
I_{peak}	33 (kA)	Calculated
I_{avg}	22 (kA)	Calculated
$t_{discharge}$	4.3 (ms)	Calculated
P_{max}	3.3 (MW)	Calculated
Efficiency	0.18 %	Calculated

The calculated output velocity of the system is predicted to match the current performance of the 16 kJ capacitor bank, which is able to accelerate projectiles to approximately 430 m/s. Having a working compulsator available for use on the EMRG Mk 1.1 will foster future pulsed power research at Cal Poly. The following figures outline the discharge performance characteristics of the compulsator over time.

In Figure 21, the top plot shows the output current of the compulsator in kA during discharge. The output curve for current visibly seems to correlate in shape with other discharge curves for current seen in other papers. The middle plot shows the decay in voltage during discharge, which is directly related to the loss in mechanical energy as the rotor's rotational velocity decays. The bottom plot shows the output power of the compulsator during discharge. Peak power is reached a third of the way

through discharge, when the voltage is still rather high and when current is approaching the average discharge current.

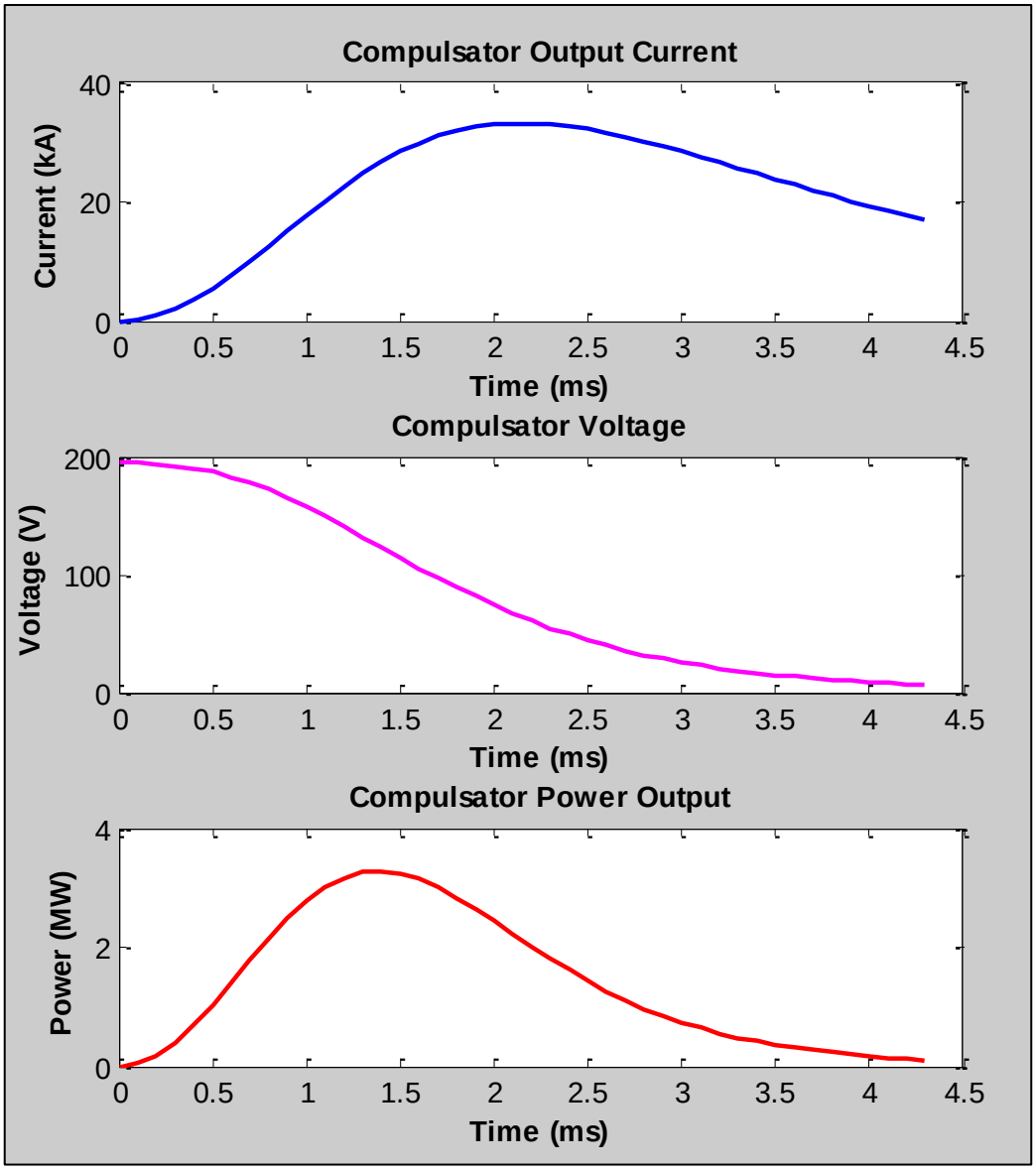

Figure 21: Discharge Simulation Results for Output Current, Voltage, and Power

Figure 22 contains plots that show the kinematic performance of the railgun and compulsator during discharge. The top plot shows the change in the projectile's position and velocity as it accelerates down the railgun barrel. The red square denotes that the projectile has reached the end of the .762m

long barrel, and at this point the simulation. Superimposed on the same plot is the velocity of the projectile while it accelerates down the railgun barrel. An additional plot showing the acceleration change during discharge will be shown and discussed later on.

The bottom plot in Figure 22 shows the change in kinetic energy stored in the rotor during discharge. The blue curve shows a decrease in RPM of the rotor speed. The green curve shows the change in stored mechanical energy remaining in the rotor, which decreases dramatically as the rotor speed decelerates from the electromechanical interaction in the system. It is important to note that the compulsator will still have a residual RPM of approximately 160 RPM after discharge; which is when the brake will be used to completely stop the rotor's motion.

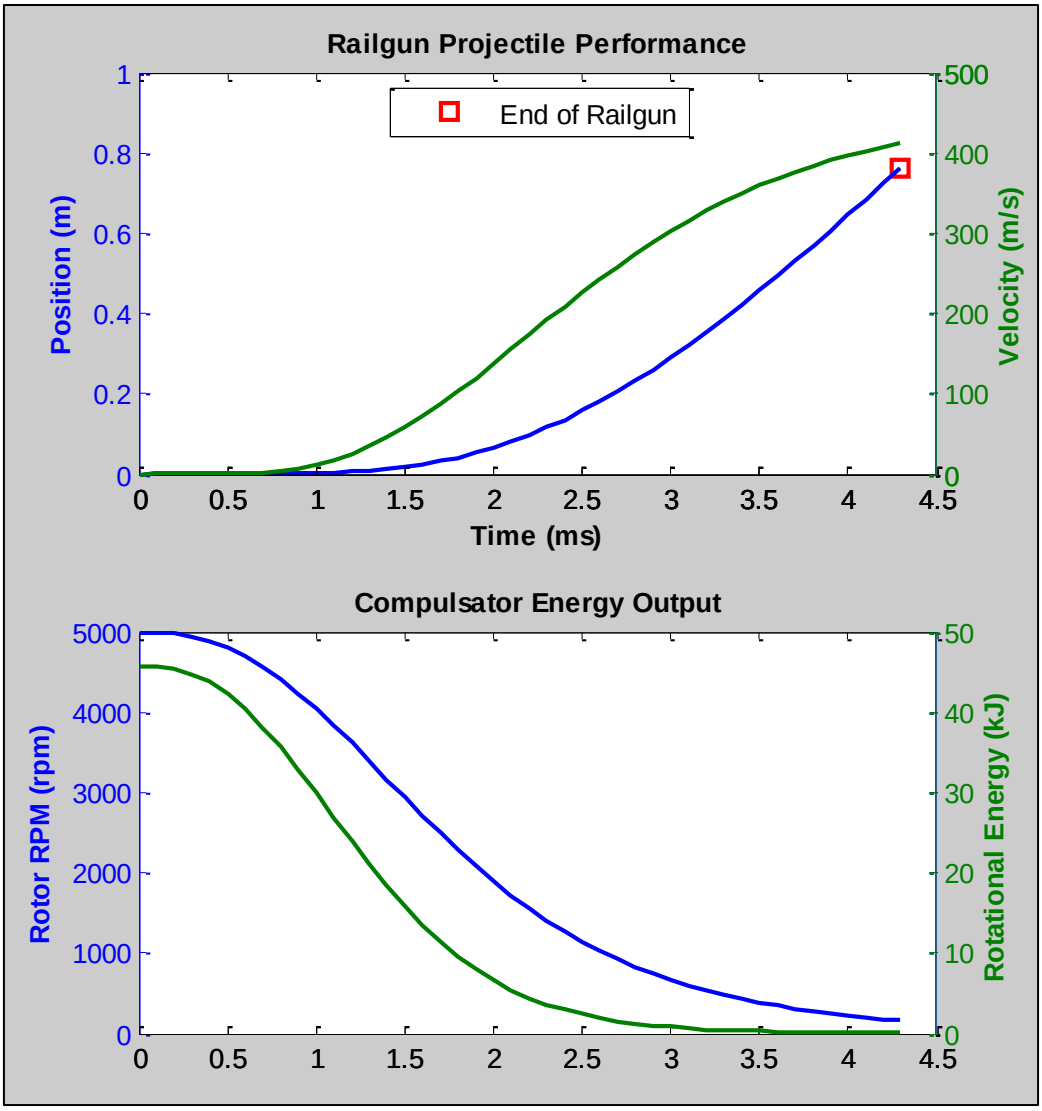

Figure 22: Discharge Simulation Results for Projectile Performance and Energy Loss in the Compulsator

The acceleration seen by the projectile during discharge is a kinematic parameter worth examining. High accelerations down the rails can induce extremely high stresses on a projectile, depending on the magnitude of the projectile's mass and acceleration seen during discharge. In the case of this project, a 1g solid aluminum projectile faces negligible stresses and there is no need to be concerned for the forces seen since there is no embedded payload. Larger railgun systems looking into embedding payloads within the projectile might have to take stresses caused from acceleration into account when selecting materials for their projectiles. A variety of applications for compulsators exist in

a variety of fields [25, 26, 3]. A plot of the acceleration seen by the projectile is included in Figure 23 below. The values for acceleration were calculated by using the kinematic equations at each time step from the data generated by the discharge simulation model.

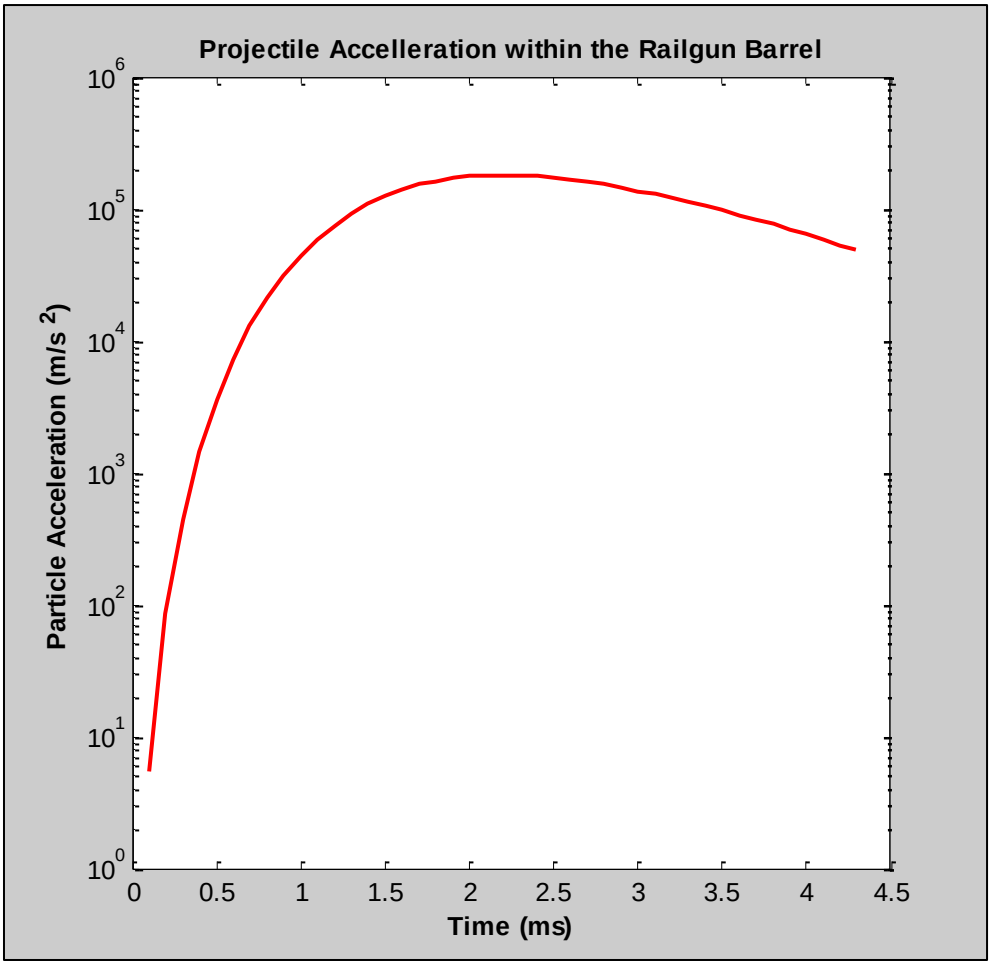

Figure 23: Discharge Acceleration performance of the 1g Aluminum projectile within the Railgun Barrel

As mentioned above in Table 4, the calculated performance of the entire compulsator-railgun system will have a supposed efficiency of 0.18%. This efficiency is calculated by examining the total initial energy stored in the rotor prior to discharge, and comparing that to the final kinetic energy of the projectile as it leaves the barrel. A plot that visualizes the conservation of energy and how the energy flows through the system is included below in Figure 24.

The green line represents the total kinetic energy that is stored in the spinning rotor during discharge; this curve is identical to the green curve in the bottom plot of Figure 22. The blue line represents the electrical energy delivered to the railgun from the compulsator during discharge. The red line is the kinetic energy of the projectile as it increases in velocity down the barrel. Lastly, the dashed black line is the summation of all three curves, and is included for clarity to show that throughout the entire discharge, energy is being conserved across the system. Because of energy losses during discharge, the rotor (green) should have the highest peak magnitude for energy, followed by the railgun (blue), and the projectile (red) should have the lowest peak magnitude for energy throughout discharge. The total system efficiency is calculated by comparing the final point on the red curve to the initial point on the green curve.

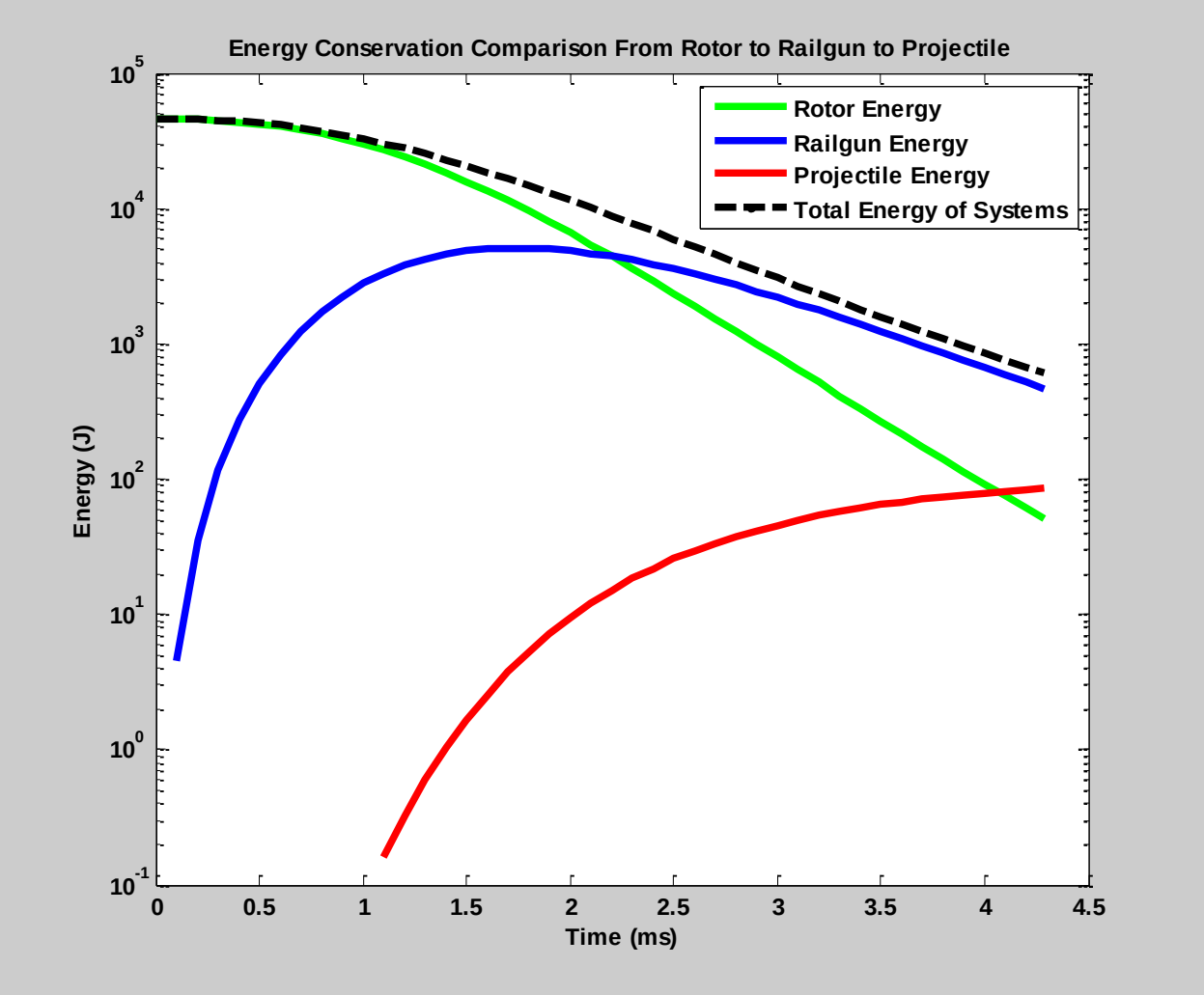

Figure 24: Conservation of energy visualized with the changes in energy during discharge between the rotor, railgun, and projectile.

The above plots showcase the calculated performance of this compulsator-railgun system. Once laboratory testing on the finished compulsator begins, comparing the experimental results with this model will occur. If the compulsator performs anywhere close to the above results, the author would consider the compulsator project a great success. As long as the finished system is able to generate voltage and move the projectile down the EMRG Mk 1.1 barrel, the author would still consider the project a partial success.

4.0 Conclusion

4.1. Current Project Status

As of mid-November 2012, the Cal Poly Compulsator is still undergoing final machining on smaller internal components. Significant work remains to assemble the rest of the internal components of the rotor section. Additionally, a variety of tasks for the external support structure, and data acquisition have yet to be started. Final assembly and the testing of the completed system is expected to occur in late-April 2013 to early May 2013.

4.2. Lessons Learned

Working on interdisciplinary projects is a very rewarding experience to have at the undergraduate level, and the opportunity to participate in any such project should always be pursued by students if the option exists. The following section contains a few anecdotal lessons learned related to this project that are applicable to any technical, group project.

4.2.1. Teamwork and Collaboration

In order to minimize a large number of group project delays and save a lot of frustration, it is very important to first focus on the people aspect of a technical project. Interdisciplinary projects, like this one, require a team of people with different technical backgrounds. Not everyone is an expert on everything, accepting this fact early on a group project when working with new people will be very useful in any similar situation. The time it took to select the final system architecture and design probably would have been reduced by several weeks, which for a student project where a quarter is ten weeks is very significant.

4.2.2. Materials Selection & Systems Engineering

Systems-level thinking coupled with budget-conscious decisions on materials selection and acquisition is important for both low-budget student projects and tight-deadline industry projects. The steel end plates caused a variety of machining delays due to the limited capability of both equipment

and team members with CNC experience. Multiple weeks of delays leading to an eventual contracting out of the completed machining of the steel plates severely impacted the original delivery schedule planned for the Compulsator (June 2012). Purchasing aluminum plates of a larger thickness perhaps 1.5-2 inches would have been much easier to machine with only a slight increase in cost of materials. However, no room remained in the budget for such a design change after the machining issues first came up, as well as redesigns on shafting and bearings would have had to occur. Effectively selecting the material of a chosen component by trading between machinability, cost, and system integrity can minimize unforeseen errors in a project down the road.

4.2.3. Materials Acquisition

The usual best-practices related to cutting material regularly mention measuring multiple times before making any cut. The same can be said when comparing product specifications. Before purchasing anything for a project, always clarify the exact purpose of a component, have all relevant a component and verify every specification. If anything seems unclear from the distributor's documentation, always contact them for more information before purchase. Following the above will reduce the chance of ordering an incorrect or irrelevant part. Fortunately, the team was able to engineer solutions that utilized all ordered materials in a successful manner. However, the time taken to find these solutions absorbed time that was meant to advance the work of the project and led to a few weeks of delays. Unforeseen issues will always arise on any project. The reason a lot of creative solutions related to the permanent magnets and the rotor winding scheme were able to be resolved is because the ordered materials were close to raw-goods, and could be reconfigured.

4.2.4. Manufacturing

When working on a project that involves extensive fabrication, a lot of proper planning must be put in place in order to stay on schedule. Reviewing CAD models and drawings with relevant team members and whoever is responsible for machining will allow for their input to modify changes to a

model that can simplify the manufacturing. Campus fabrication resources are typically in high demand, so communicating amongst team members to reserve equipment ahead of time can make the difference in being able to machine a part on the day you planned versus the next day.

4.2.5. Research

One of the goals of this paper is to provide a bridge between technical conference papers and a reader who is new to the field of compulsators and railguns. The best advice for anyone when working on a topic outside their existing knowledgebase is to become as well-read as possible. If there is information to be gleaned from portions of textbooks, find it, read it, and save it for later reference. When the published knowledgebase mostly is comprised of conference papers, find and download as many papers as possible. Read and reread them multiple times, try and implement the mathematics shown in papers to learn the material firsthand. It took about eight months of research and several attempts before the analysis shown in this paper was reached. All members on a project should be putting in a minimum baseline of research into a new field of study, as a lot of previous lessons or decisions behind design choices can be found in previously published research.

4.2.6. Documentation

Clear and functional documentation is key to any project. When working in a team environment, clearly presenting your assumptions and processes used to achieve calculated results is very important. It provides your peers with additional means to constructively ensure that you did not overlook something. Most importantly your assumptions, method, and results must make sense and be agreed upon by the rest of your team in that order of importance. Additionally, leaving behind clear drawings for machined parts and listing out suppliers is useful for anyone who might do follow up work on a project after the original team members have moved on. Eventually, the procedures taken to assemble the finished compulsator and the operational testing procedures will be well documented for both training and safety purposes to assist future students.

4.3. Future Work

At this stage in time, the future work related to the compulsator will be focused on completing manufacturing, assembly, and getting the compulsator ready for integrated testing with EMRG Mk. 1.1. After testing, a comparison of the experimental discharge performance of the compulsator will occur with the results from the theoretical analysis outlined previously in this paper. This work will be the author's focus as part of their Master's Thesis. Once the compulsator has been setup to handle frequent testing on a regular basis, there is room for a lot of follow up research in some of the following areas:

- Rotordynamic analysis of the rotor during operation and discharge
- Electromagnetic Analysis of the compulsator
- Modular upgrades to the stator section
- Model-Based Systems Engineering of the existing compulsator system
- Multidisciplinary Design Optimization for future compulsator work

5.0 References

[1] A. C. Tribble, The Space Environment: Implications for Spacecraft Design, Princeton: Princeton University Press, 2003.

[2] J. Maniglia, J. Smiroldo, A. Westfall and G. Zohar, "Design, Fabrication, and Testing of an Electromagnetic Railgun for the repeated testing and simulation of Orbital Debris Impacts," California Polytechnic State University, San Luis Obispo, 2011.

[3] J. Kitzmiller, S. Pratap and M. Driga, "An Application Guide for Compulsators," in *11th EML Technology Symposium*, Saint-Louis, France, 2002.

[4] M. Spann, S. Pratap, M. Werst, W. Walls and C. Fulcher, "Compulsator Research at the University of Texas at Austin -- an Overview," in *4th Symposium on Electromagnetic Launch Technology*, Austin, TX, 1988.

[5] W. Weldon, M. Driga and H. Woodson, "Compensated Pulsed Alternator". United States of America Patent 4,200,831, 29 April 1980.

[6] D. Putley, R. C. McLachlan and D. A. Hughes, "Design Considerations for Compulsator Driven Railguns," *IEEE Transactions on Magnetics, Vol. 25, No. 1,* pp. 474-479, January 1989.

[7] W. Bird, H. Woodson and H. Rylander, "Detailed Design, Fabrication and Testing of an Engineering Prototype Compensated Pulsed Alternator," Center for Electromechanics, The University of Texas at Austin, Austin, 1980.

[8] W. Walls, M. Spann, S. Pratap, D. Bresie, W. Brinkman, J. Kitzmiller, J. Herbst, H. Liu, S. Manifold and B. Rech, "Design of a Self-Excited, Air-Core Compulsator for a Skid-Mounted, Repetitive Fire 9 MJ Railgun System," in *4th Symposium on Electromagnetic Launch Technology*, Austin, TX, 1988.

[9] Q. Zhang, S. Wu, C. Yu, S. Cui and L. Song, "Design of a Model-Scale Air-Core Compulsator," *IEEE Transactions on Plasma Science,* vol. 39, no. 1, pp. 346-353, 2011.

[10] W. Walls, "Advanced Compulsator Topologies and Technologies," The University of Texas at Austin, Austin, 2002.

[11] I. R. McNab, "Megampere Pulsed Alternators for Large EM Launchers," in *2006 IEEE International Conference on Megagauss Magnetic Field Generation and Related Topics*, Austin, TX, 2006.

[12] W. Bird, M. Driga, D. Mayhall and M. Brennan, "Pulsed Power Supplies for Laser Flashlamps," Center for Electromagnetics - The University of Texas at Austin, Austin, TX, 1978.

[13] C. Ye, K. Yu, Z. Lou and Y. Pan, "Investigation of Self-Excitation and Discharge Processes in an Air-Core Pulsed Alternator," *IEEE Transactions on Magnetics,* vol. 46, no. 1, pp. 150-154, 2010.

[14] X. Liu, K. Yu, S. Yang, C. Ye, X. Wang and Y. Pan, "Electromagnetic Analysis of a Permanent Magnet Compulsator (PMCPA)," in *Universities Power Engineering Conference 2006*, Wuhan, 2006.

[15] J. F. O'Hara III, "Ignitron Trigger Circuit," California Polytechnic State University, San Luis Obispo, CA, 2012.

[16] B. Bennett, "Compulsator Design for Electromagnetic Railgun System," California Polytechnic State University, San Luis Obispo, 2012.

[17] A. Miller, E. Pratt and J. Terry, "Compulsator Final Report," California Polytechnic State University, San Luis Obispo, 2012.

[18] M. Driga, S. Pratap and W. Weldon, "Advanced Compulsator Design," in *4th IEEE Symposium on Electromagnetic Launch Technology*, Austin, 1988.

[19] L. Li, W. Wu and Y. Xiong, "Study of Two-Phase Passive Compulsator," *IEEE Transactions on Magnetics,* vol. 39, no. 1, pp. 348-252, January 2003.

[20] Y. Xiong, L. Li and Z. Ma, "Analysis and Modeling of the Active Compulsator," *IEEE Transactions on Magnetics,* vol. 39, no. 1, pp. 394-397, January 2003.

[21] M. Giesselmann and D. Eccleshall, "Modeling of a Compulsator and Railgun System," *IEEE Transactions on Magnetics,* vol. 37, no. 1, pp. 129-134, January 2001.

[22] D. Putley, "Analysis and Modelling of the Culham Experimental Compulsator," in *6th IEEE Pulsed Power Conference*, 1987.

[23] W. Hayt and J. Buck, Engineering Electromagnetics, 6th ed., New York: McGraw-Hill Higher Education, 2000, pp. 369-376.

[24] "Energy Storage System," Kumamoto University 21st Century COE Program, 2004. [Online]. Available: http://pps.coe.kumamoto-u.ac.jp/streaming/PulsedPower/generator/energy%20storage1.htm. [Accessed 15 May 2012].

[25] I. McNab and F. Beach, "Present and Future Naval Applications for Pulsed Power," in *IEEE Pulsed Power Conference*, Austin, 2005.

[26] R. M. Jones, "Electromagnetically Launched Micro Spacecraft for Space Science Mission," *AIAA Journal of Spacecraft and Rockets,* vol. 26, no. 5, p. 338, 1989.

[27] J. Kitzmiller, S. Pratap and M. Driga, "An Application Guide for Compulsators," in *11th Electromagnetic Launch Technology Symposium*, Saint-Louis, France, 2002.

6.0 Appendix

Appendix A: Matlab code of Compulsator Discharge

Included below is the code used to generate the results discussed in this paper. It has been left in a raw form that will allow for immediate use by any interested party. The code is separated into three files:

- **System_Setup.m**
  - This runs all of the analysis. System parameters for the compulsator, railgun, and projectile are input here. Plotting of results also occurs within this file.
- **CPA_EMRG.m**
  - This is the ode45 function that propogates the system of differential equations forward in time through the discharge event.
- **Event_RailEnd.m**
  - This stops the simulation when the projectile leaves the barrel of the railgun

As long as all three files are in the same directory, running System_Setup.m is all that is necessary.

System_Setup.m

```
clear all
close all
clc
format compact
%% Setup of Variables
%Collin MacGregor
%ctmacgre@calpoly.edu
%California Polytechnic State University, San Luis Obispo, CA

%This code runs analytically solves for the discharge performance of a
%compulsator/railgun system utilizing a state-space approach.

% Solve for resistance of each winding
n = 10; % Wire gauge used
nw = 1; % # of parallel conductors in the winding

global Np Npp Ncp B Dr Lr Jr Lmin Lmax Rho Rcp Ro Lo Rrg Xrg RPrg LPrg Ph_1
Ph_2 Mp dt
Np  = 8;       %Number of Poles in the System
Npp = 4;        %Number of Pole Pairs in Rotor
Ncp = 4;       %Number of conductors per pole on rotor
B   = .45;       %Magnetic Field Strength Density (T)
Dr  = 8*.0254;  %Diameter of Rotor (m)
Lr  = 10*.0254; %Length of Rotor (m)
Jr  = 1140*6.452E-4*.454; %Inertia of Rotor (kg-m^2)
Lmin= 1e-5;     %Minimum Inductance of Compulsator (H)
Lmax= 1*1e-5;     %Maximum Inductance of Compulsator (H)
Rho = .5*(Lmax/Lmin - 1); %Compulsator Inductance Modulus
Rcp = .000375; %Resistance of Compulsator Rotor Winding Phase (Ohms)
Ro  = 1e-6;     %Resistance of connecting busbar/switching (Ohms)
Lo  = 1e-6;        %Inductance of connecting busbar/switching (H)
Rrg = 3.2104e-004; %Resistance of the Railgun (Ohms)
Xrg = 2.5*0.3048; %Length of Railgun Rails (m)
RPrg= Rrg*Xrg;  %Resistance Gradient of Rails (Ohms/m)
LPrg= 3.2712e-007; %Inductance Gradient of Rails (H/m)
Ph_1= 0;        %Electrical Phase Angle "1" (rad)
Ph_2= pi;     %Electrical Phase Angle "2" (rad)
Mp  = .001;     %Mass of Particle (kg)
dt = 1e-4;      % Time step size (s)

%Other Variables
RPM0= 5000;     %Initial RPM of the Rotor (rpm)
Wr0 = RPM0/60*2*pi; %Angular Velocity of Rotor (rad/s)
x0  = 0;        %Initial Particle Position (m)
Vp0 = 0;        %Initial Particle Velocity (m/s)
I_0 = 0;        %Initial Current of Compulsator (A)

%% SETUP & RUN ODE45

t0  = 0;        %Initial Time (s)
tf  = 10e-3;     %Final Simulation Time (s)
```

```
IVP = [Wr0; x0; Vp0; I_0];
ODE_FUN = @CPA_EMRG;
% tspan = linspace(0,3e-3,1e3);
tspan = t0:dt:tf;
options = odeset('AbsTol',1e-8,'RelTol',1e-8,'Events',@Event_RailEnd);

[Tout, dIVP] = ode45(ODE_FUN,tspan,IVP,options);

Wout = dIVP(:,1);
Xout = dIVP(:,2);
Vout = dIVP(:,3);
Iout = dIVP(:,4);

%% Manipulate output Data
Vtip_out= Wout*Dr/2;
We_out = Wout*Npp/(2*pi);
Volt_out  = Np*Ncp*Lr*B*Vtip_out;%.*sin(We_out.*Tout);
Wrpm_out = Wout*60/2/pi;
Er_out = .5*Jr*Wout.^2;
Pwr_out = Volt_out.*Iout;
Velocity = Vout(end);
RPM_dropP = (1-Wout(end)/Wout(1))*100;
Tend = Tout(end);

%Energy At end Calculation
Eo_s = .5*Jr*Wout(1)^2; %J
Ef_p = .5*Mp*Velocity^2; %J

P_accel = zeros(length(Xout),1);
for j = 2:length(Xout)
    P_accel(j) = (Vout(j)^2-Vout(j-1)^2)/(2*(Xout(j)-Xout(j-1)));
end

F_accel = Mp*P_accel; %kgs

CP_E_Out = Tout.*Pwr_out; %Energy Discharged by Compulsator (J)
P_E_Out = .5*Mp*Vout.^2; %Projectile Energy (J)


%% Plotting
subplot(3,1,1)
plot(Tout*1e3,Iout/1e3,'linewidth',2)
xlabel 'Time (ms)'
ylabel 'Current (kA)'
title 'Compulsator Output Current'

subplot(3,1,2)
plot(Tout*1e3,Volt_out,'m','linewidth',2)
xlabel 'Time (ms)'
ylabel 'Voltage (V)'
title 'Compulsator Voltage'
```

```
subplot(3,1,3)
plot(Tout*1e3,Pwr_out/1e6,'r','linewidth',2)
xlabel 'Time (ms)'
ylabel 'Power (MW)'
title 'Compulsator Power Output'

figure (2)
subplot(2,1,1)
plot(Tout(end)*1e3,Xrg,'rs','linewidth',2)
hold on
plotyy(Tout*1e3,Xout,Tout*1e3,Vout)
[AX,H1,H2] = plotyy(Tout*1e3,Xout,Tout*1e3,Vout,'plot');
set(get(AX(2),'Ylabel'),'String','Velocity (m/s)')
set(get(AX(1),'Ylabel'),'String','Position (m)')
set(H1,'linewidth',2);
set(H2,'linewidth',2)
xlabel('Time (ms)')
legend('End of Railgun','location','north')
title('Railgun Projectile Performance')

subplot(2,1,2)
plotyy(Tout*1e3,Wrpm_out,Tout*1e3,Er_out)
[AXo,H1o,H2o] = plotyy(Tout*1e3,Wrpm_out,Tout*1e3,Er_out/1e3,'plot');
set(get(AXo(2),'Ylabel'),'String','Rotational Energy (kJ)')
set(get(AXo(1),'Ylabel'),'String','Rotor RPM (rpm)')
set(H1o,'linewidth',2);
set(H2o,'linewidth',2)
title 'Compulsator Energy Output'

figure(3)
semilogy(Tout*1e3,P_accel,'r','linewidth',2)
xlabel 'Time (ms)'
ylabel 'Particle Acceleration (m/s^2)'
title 'Projectile Accelleration within the Railgun Barrel'

%This is to prevent drastic 10^-15 on semilog plots
ind = min(find(P_E_Out > .1));
Tot_E = Er_out+CP_E_Out+P_E_Out;

figure(4)
semilogy(Tout*1e3,Er_out,'g','linewidth',2)
hold on
plot(Tout*1e3,CP_E_Out,'b','linewidth',2)
plot(Tout(ind:end)*1e3,P_E_Out(ind:end),'r','linewidth',2)
plot(Tout*1e3,Tot_E,'k--','linewidth',2)
hold off
xlabel 'Time (ms)'
ylabel 'Energy (J)'
legend('Rotor Energy','Railgun Energy','Projectile Energy','Total Energy of
Systems')
title('Energy Conservation Comparison From Rotor to Railgun to Projectile')

disp (['Voltage @T=0 = ',num2str(Volt_out(1)),' (V)'])
% disp (['Final Voltage= '
```

```
disp (['End Velocity = ',num2str(Vout(end)),' (m/s)'])
disp (['Peak Current = ',num2str(max(Iout)/1e3),' (kA)'])
disp (['Avg Current  = ',num2str(mean(Iout/1e3)),' (kA)'])
disp (['Peak Power   = ',num2str(max(Pwr_out)/1e6),' (MW)'])
disp (['Pulse Time   = ',num2str(Tout(end)*1e3), ' (ms)'])
disp (['Efficiency   = ',num2str((Ef_p/(Er_out(1)-Er_out(end)))*100),' %'])
```

CPA_EMRG.m

```
function [ dIVP ] = CPA_EMRG( T, IVP )
global Np Npp Ncp B Dr Lr Jr Lmin Lmax Rho Rcp Ro Lo Rrg Xrg RPrg LPrg
Ph_1 Ph_2 Ph_3 Ph_4 Mp dt
%
Np;Npp;Ncp;B;Dr;Lr;Jr;Lmin;Lmax;Rho;Rcp;Ro;Lo;Rrg;Xrg;RPrg;LPrg;Ph_1;P
h_2;Mp;dt;
%This function analytically solves for the state space model of the
%Compulsator/Railgun system.

Wr = IVP(1);        %Angular Velocity of Rotor (rad/s)
x  = IVP(2);        %Position of projectile (m)
Vp = IVP(3);        %Velocity of projectile (m/s)
I  = IVP(4);        %Current of Compulsator (A)

%% Calculate State 1: Change in Angular Velocity
Er  = .5*Jr*Wr^2;   %Rotational Energy Stored in Rotor (J)
Vtip= Wr*Dr/2;      %Tip Speed of Rotor Edge (m/s)
Vo  = Np*Ncp*Lr*B*Vtip; %EMF Voltage of Rotor (V)
We  = Wr*Npp/(2*pi);%Electrical Frequency of Machine (1/s)
V   = Vo*sin(We*T); %Voltage of Machine over time (V)

% dWr = 0;
dWr = -sqrt(((2*V*I)/Jr)*dt)/dt;
%   dWr   =   (-V*I)   /   sqrt((2/Jr)*(Er-V*I*2.7227e-005));   %Angular
Acceleration (rad/s^2)

%% Calculate State 3: Change in Particle Velocity

dVp = (LPrg*I^2) / (2*Mp); %Particle Accelleration (m/s^2)

%% Calculate State 2: Change in Particle Position

dx  = Vp; %Particle Velocity (m/s)

%% Calculate State 4: Change in Compulsator Current
%Phase-1
L1   = Lmin*Rho*sin(We*T-Ph_1);
Top1  = V  -  I*(Rcp  +  Ro  +  RPrg*x)  +  I*(We*Lmin*Rho*sin(We+Ph_1)  -
LPrg*Vp);
Bot1 = Lmin*(1+Rho) + L1 + LPrg*x + Lo;

L1b   = Lmin*Rho*sin(We*T-Ph_1);
Top1b  = V  -  I*(Rcp  +  Ro  +  RPrg*x)  +  I*(We*Lmin*Rho*sin(We+Ph_1)  -
LPrg*Vp);
Bot1b = Lmin*(1+Rho) + L1b + LPrg*x + Lo;

L1c   = Lmin*Rho*sin(We*T-Ph_1);
```

```
Top1c = V - I*(Rcp + Ro + RPrg*x) + I*(We*Lmin*Rho*sin(We+Ph_1) -
LPrg*Vp);
Bot1c = Lmin*(1+Rho) + L1c + LPrg*x + Lo;

L1d   = Lmin*Rho*sin(We*T-Ph_1);
Top1d = V - I*(Rcp + Ro + RPrg*x) + I*(We*Lmin*Rho*sin(We+Ph_1) -
LPrg*Vp);
Bot1d = Lmin*(1+Rho) + L1d + LPrg*x + Lo;

%Phase-2
L2   = Lmin*Rho*sin(We*T-Ph_2);
Top2 = V - I*(Rcp + Ro + RPrg*x) + I*(We*Lmin*Rho*sin(We+Ph_2) -
LPrg*Vp);
Bot2 = Lmin*(1+Rho) + L2 + LPrg*x + Lo;

L2b   = Lmin*Rho*sin(We*T-Ph_2);
Top2b = V - I*(Rcp + Ro + RPrg*x) + I*(We*Lmin*Rho*sin(We+Ph_2) -
LPrg*Vp);
Bot2b = Lmin*(1+Rho) + L2b + LPrg*x + Lo;

L2c   = Lmin*Rho*sin(We*T-Ph_2);
Top2c = V - I*(Rcp + Ro + RPrg*x) + I*(We*Lmin*Rho*sin(We+Ph_2) -
LPrg*Vp);
Bot2c = Lmin*(1+Rho) + L2c + LPrg*x + Lo;

L2d   = Lmin*Rho*sin(We*T-Ph_2);
Top2d = V - I*(Rcp + Ro + RPrg*x) + I*(We*Lmin*Rho*sin(We+Ph_2) -
LPrg*Vp);
Bot2d = Lmin*(1+Rho) + L2d + LPrg*x + Lo;

%Summation of Phase outputs
dI  = Top1/Bot1 + Top2/Bot2 + + Top1b/Bot1b + Top2b/Bot2b + ...
      Top1c/Bot1c + Top2c/Bot2c + Top1d/Bot1d + Top2d/Bot2d;

dIVP = [dWr; dx; dVp; dI];

end
```

Event_RailEnd.m

```
function [value,isterminal,direction] = Event_RailEnd( t, y )
global Np Npp Ncp B Dr Lr Jr Lmin Lmax Rho Rcp Ro Lo Rrg Xrg RPrg LPrg
Ph_1 Ph_2 Ph_3 Ph_4 Mp dt

Np;Npp;Ncp;B;Dr;Lr;Jr;Lmin;Lmax;Rho;Rcp;Ro;Lo;Rrg;Xrg;RPrg;LPrg;Ph_1;P
h_2;Ph_3;Ph_4;Mp;dt;

%Stop integration when particle leaves the rails
v1 = y(2) - Xrg;
value       = v1;
isterminal  = 1;
direction   = 0;

end
```

Appendix B: Energy Discharge Equation Derivation

Work done to reach this equation was primarily contributed by Jeff Maniglia, a graduate student assisting on the project.

(1) $$\boldsymbol{E_r} = \frac{\mathbf{1}}{\mathbf{2}} * \boldsymbol{J} * \boldsymbol{w_r}^{\mathbf{2}}$$

(2) $$\frac{\boldsymbol{\partial E_r}}{\boldsymbol{\partial t}} = \boldsymbol{V} * \boldsymbol{I} * \boldsymbol{dt}$$

(3) $$\frac{\boldsymbol{\partial E_r}}{\boldsymbol{\partial t}} = \boldsymbol{E_{r-old}} - \boldsymbol{E_{r-new}}$$

(4) $$\boldsymbol{V} * \boldsymbol{I} * \boldsymbol{dt} = \frac{\mathbf{1}}{\mathbf{2}} * \boldsymbol{J} * (\boldsymbol{w_{r-old}} - \boldsymbol{w_{r-new}})^{\mathbf{2}}$$

(5) $$\Delta \boldsymbol{w_r} = \boldsymbol{w_{r-old}} - \boldsymbol{w_{r-new}}$$

(6) $$\boldsymbol{V} * \boldsymbol{I} * \boldsymbol{dt} = \frac{\mathbf{1}}{\mathbf{2}} * \boldsymbol{J} * \Delta \boldsymbol{w_r^2}$$

(7) $$\Delta \boldsymbol{w_r} = \sqrt{\frac{\mathbf{2} * \boldsymbol{V} * \boldsymbol{I}}{\boldsymbol{J}} \boldsymbol{dt}}$$

(8) $$\frac{\Delta \boldsymbol{w_r}}{\boldsymbol{dt}} = \frac{-\sqrt{\frac{\mathbf{2} * \boldsymbol{V} * \boldsymbol{I}}{\boldsymbol{J}} \boldsymbol{dt}}}{\boldsymbol{dt}}$$

Appendix C: Bill of Raw Materials/Components with Vendor Listing, Contact Information, and Pricing

Category	Amount	Cost Per	Estimated Cost	Source / Vendor	Supplier/Contact Info	More Info
Stator Material						
Aluminum Stator Casing	1 ft	$189.00	$189.00	MetalsDepot	MetalsDepot.com	P/N T310
1.25T Magnets	40	$13.87	$554.80	MagCraft	rare-earth-magnets.com	P/N NSN0607 (packs of 4)
Aluminum bar (1"x1") for interpoles and magnet rails	2	$36.18	$72.36	MetalsDepot	MetalsDepot.com	P/N SQ31 (2x6ft bars)
Flanges for stator (1/4"x2")	1	$17.82	$17.82	MetalsDepot	MetalsDepot.com	P/N F4142 (6 ft)
Stator Mounting Nuts	1	$4.44	$4.44	McMaster	McMaster.com	P/N 9713A250 (Packs of 10)
Stator Mounting Bolts	1	$11.13	$11.13	McMaster	McMaster.com	P/N 91247A732 (pack of 10)
Interpole/Mag. Rail Bolts	5	$6.99	$34.95	McMaster	McMaster.com	P/N 92240A750 (packs of 10)
Rotor Components						
Copper Wire 10 AWG (in ft)	347.5	$0.40	$139.00	Magnets4Less	Magnet4less.com	P/N AWG10-11
Aluminum Plate (t=1/16") 12"x12"	1	$19.09	$19.09	Speedy Metals	speedymetals.com	
Steel Flywheel (8in OD) 10in length	1	$351.90	$351.90	Speedy Metals	speedymetals.com	1018 Hot Rolled
Brake side Angular contact Roller Bearing (Bore 1.1811")	1	$272.75	$272.75	McMaster	McMaster.com	P/N 2385K46
Clutch side Angular contact Roller Bearing (Bore 0.78")	1	$224.16	$224.16	McMaster	McMaster.com	P/N 2385K44
Flanges for rotor	1	$14.08	$14.08	MetalsDepot	MetalsDepot.com	P/N P114 (1"x1" 1/4" thick)
Brushes	8	$0.00	$0.00	Waiting For Quote		
Brush Holders	8	$0.00	$0.00	Waiting For Quote		
Commutator (Kirkwood 16 Bar)	1	$0.00	$0.00	Kirkwood	Donated from Kirkwood	0.7855" bore
Prime Mover Components						
16 Tooth Pinion	1	$19.14	$19.14	McMaster	McMaster.com	P/N 5172T21
48 Tooth Gear	1	$47.00	$47.00	McMaster	McMaster.com	P/N 5172T24
Studs (6" long 3/8"-16)	4	$2.00	$8.00	McMaster	McMaster.com	P/N 98750A080
Nuts (3/8"-16)	4	$0.00	$0.00	HomeDepot	Homedepot.com	3/8"-16
0.625" bearing for pinion shaft	1	$14.88	$14.88	McMaster	McMaster.com	P/N 2780T22
Friction Brake	1	$327.61	$327.61	Nexen Group	Applied Tech/805-928-1864::Quote-139642	P/N J 841600, 842100 & 842000
Magnetic Clutch	1	$294.79	$294.79	SDP-SI	SDP-SI.com	P/N S90CSC-30A1010
Pinion Shafting (5/8" OD) 2ft Length	1	$5.92	$5.92	MetalsDepot	MetalsDepot.com	P/N R258
Gear Shafting (7/8" OD) 2ft length	1	$13.58	$13.58	MetalsDepot	MetalsDepot.com	P/N R278
brake Shafting (1.25" OD) 1ft length	1	$11.46	$11.46	MetalsDepot	MetalsDepot.com	P/N R2114
Pinion Shaft Bearing (Bore .625")	1	$21.65	$21.65	McMaster	McMaster.com	P/N 8258K21
Single Phase Induction Motor	1	$380.00	$380.00	McMaster	McMaster.com	P/N 5990K23
Base Components						
Steel Mounting Bars for Stator (1 1/2"x3")	1	$130.16	$130.16	MetalsDepot	MetalsDepot.com	P/N F223 (4ft)
Endplate Bolts to Mounting Bars for Stator	2	$10.78	$21.56	McMaster	McMaster.com	P/N 90201A429 (Packs of 5)
Endplates (1ftx2ftx1in)	2	$167.02	$334.04	MetalsDepot	MetalsDepot.com	P/N P11 (1ftx2ftx1in)
5/16-18 Brake Fastener	1	$8.13	$8.13	McMaster	McMaster.com	P/N 91309A583 (*pack of 100)
Subtotal Estimated Cost	$3,543.40					
Subtotal Taxes	$0.00					
Subtotal Shipping	$17.06					
Total	$3,560.46					